iScience

CellPress
OPEN ACCESS

Article

Regulated regeneration of adipose tissue in lipodystrophic *Agpat2*-null mice partially ameliorates hepatic steatosis

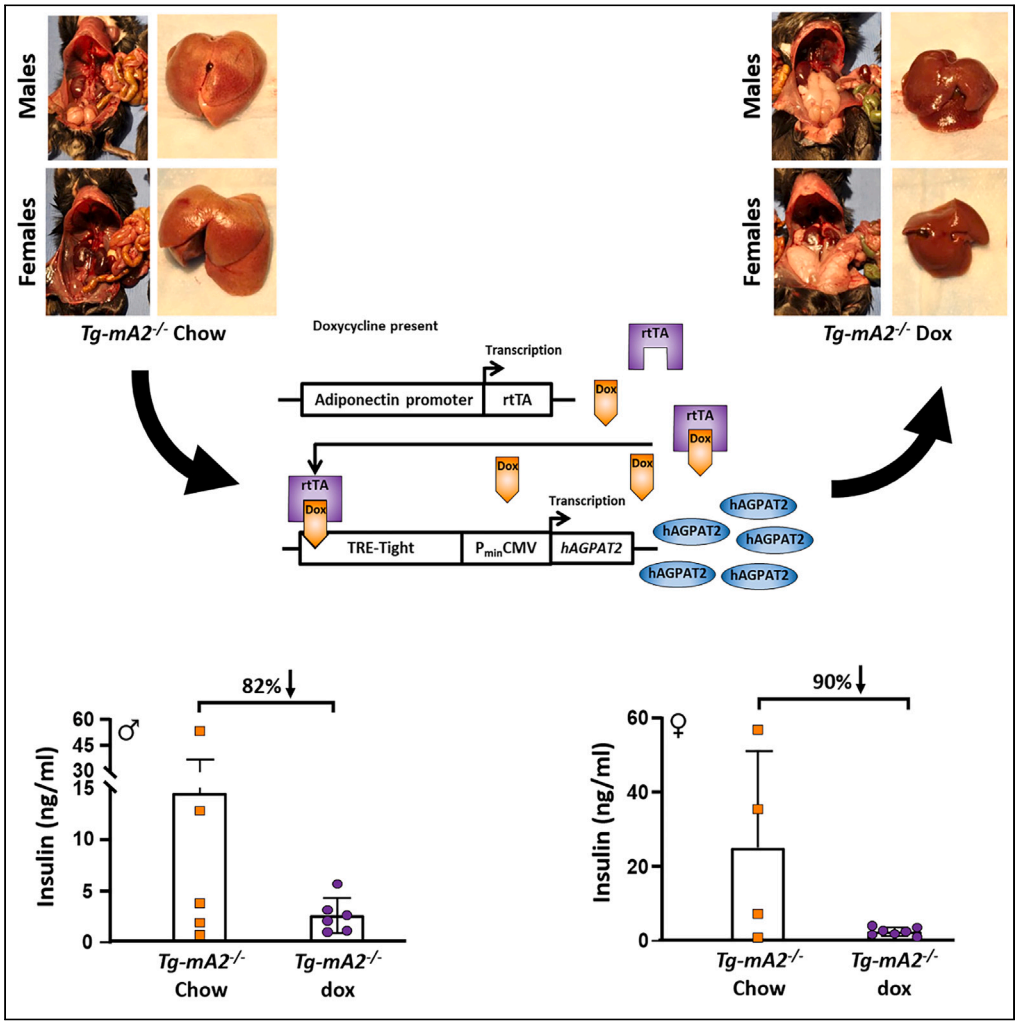

Anil K. Agarwal, Katie Tunison, Jay D. Horton, Abhimanyu Garg

anil.agarwal@utsouthwestern.edu

Highlights

Regeneration of adipose tissue in Agpat2−/− lipodystrophic mice improved hepatic steatosis

Regenerated adipose tissue decreased hepatic *de novo* lipogenesis

Fasting plasma glucose returned to near WT levels in dox-fed Tg-$^{AT\text{-}hA2}$; mA2$^{-/-}$ mice

Energy balance normalizes to WT levels in dox-fed Tg-$^{AT\text{-}hA2}$; mA2$^{-/-}$ mice

Agarwal et al., iScience 27, 109517
April 19, 2024
https://doi.org/10.1016/j.isci.2024.109517

iScience

CellPress
OPEN ACCESS

Article

Regulated regeneration of adipose tissue in lipodystrophic *Agpat2*-null mice partially ameliorates hepatic steatosis

Anil K. Agarwal,[1,2,4,*] Katie Tunison,[1,2] Jay D. Horton,[2,3] and Abhimanyu Garg[1,2]

SUMMARY

Both humans and mice with congenital generalized lipodystrophy due to AGPAT2 deficiency develop diabetes mellitus, insulin resistance, and hepatic steatosis, which have been attributed to the near total loss of adipose tissue (AT). Here, we show that regulated AT regeneration in doxycycline (dox)-fed Tg$^{-AT\text{-}hAGPAT2}$;m*Agpat2*$^{-/-}$ mice partially ameliorates hepatic steatosis at 12 weeks of age and causes reduced expression of genes involved in hepatic *de novo* lipogenesis despite partial (~30–50%) AT regeneration compared to that in wild-type mice. Compared to chow-fed Tg$^{-AT\text{-}hAGPAT2}$;m*Agpat2*$^{-/-}$ mice, those fed dox diet had markedly reduced serum insulin levels, suggesting an improvement in insulin resistance. Interestingly, the fasting plasma glucose levels in dox-fed Tg$^{-AT\text{-}hAGPAT2}$;m*Agpat2*$^{-/-}$ mice were no different than those in chow-fed wild-type mice. Indirect calorimetry revealed normalization in the energy balance of dox-fed Tg$^{-AT\text{-}hAGPAT2}$;m*Agpat2*$^{-/-}$ mice compared to that in chow-fed mice. This study's findings suggest that partial AT regeneration in lipodystrophic mice can ameliorate metabolic derangements.

INTRODUCTION

Hepatic steatosis is a cardinal feature of almost all types of partial or generalized lipodystrophies in humans where there is substantial loss of body fat. The severity of hepatic steatosis, commonly known as nonalcoholic fatty liver disease (NAFLD), correlates with the extent of fat loss. Reduced or absent adipose tissue (AT) in lipodystrophy[1–3] and excess of AT in obesity[4] result in several metabolic abnormalities including NAFLD, which some investigators refer to as steatotic liver disease or metabolic dysfunction-associated steatotic liver disease.[5,6] Currently, there is an ongoing debate on how to classify the clinical variants of hepatic steatosis[7,8] before new nomenclature for NAFLD can be adopted.

This study stems from our previous observation made while analyzing the murine model of congenital generalized lipodystrophy type 1 (CGL1) in which the 1-acylglycerol-3-phosphate O-acyltransferase 2 (*Agpat2*) gene was deleted.[9] AGPAT2 converts lysophosphatidic acid (LPA) to phosphatidic acid (PA) in the second step of the glycerol-3-phosphate (G-3-P) pathway.[10] The *Agpat2*$^{-/-}$ murine model closely recapitulates many features of the common forms of human nonalcoholic hepatic steatosis.[11] Another murine model exists, *ob/ob*, that similarly develops hepatic steatosis, albeit in the presence of an excess of AT (obesity). It is interesting to note that although both murine models develop hepatic steatosis because of a lack of leptin, the causes of leptin deficiency are different. In *Agpat2*$^{-/-}$ mice, lack of AT results in leptin deficiency, whereas in *ob/ob* mice, a mutation in the leptin (*Lep*) gene results in non-functional leptin.

AT is normally the major site of triacylglycerol (TAG) synthesis and storage, whereas tissues like the liver and skeletal muscles are not. Any increase in TAG levels in the liver or skeletal muscles results in metabolic disruption.[12] Several metabolic pathways are involved in TAG biosynthesis, with the two most commonly known pathways being the G-3-P, also known as the Kennedy pathway, in which G-3-P is sequentially acylated and dephosphorylated to produce TAG, and the monoacylglycerol (MAG) pathway, in which MAG is acylated to diacylglycerol (DAG), which is then further acylated to TAG as in the G-3-P pathway.[13,14] The MAG pathway is believed to be prominent in re-esterification of hydrolyzed TAG. There are three isoforms of monoacylglycerol acyltransferases (*Mogat* 1–3). *Mogat1* is primarily expressed in the intestines (enterocytes of the small intestines) followed by the stomach and kidney,[15] as well as in conditions of liver pathology, such as hepatic steatosis.[9]

The findings described here are part of a larger study where we demonstrate the regeneration of AT in *Agpat2*$^{-/-}$ mice,[16] overexpression of human *AGPAT2* (h*AGPAT2*) specifically in AT, and the effect of AGPAT2 on TAG synthesis in AT.[17] To investigate this, we constructed a transgenic murine model expressing h*AGPAT2* specifically in AT, driven by the adiponectin promoter, and regulated by doxycycline (dox)[16] (Tg-$^{AT\text{-}hA2}$;mA2$^{-/-}$) (Figures S1A and S1B). Using this strategy, we observed the regeneration of AT, albeit at a reduced quantity (~30–50%),

[1]Section of Nutrition and Metabolic Diseases, Division of Endocrinology, Department of Internal Medicine, UT Southwestern Medical Center, Dallas, TX 75390, USA
[2]Center for Human Nutrition, UT Southwestern Medical Center, Dallas, TX 75390, USA
[3]Department of Molecular Genetics, UT Southwestern Medical Center, Dallas, TX 75390, USA
[4]Lead contact
*Correspondence: anil.agarwal@utsouthwestern.edu
https://doi.org/10.1016/j.isci.2024.109517

compared to that in wild-type (WT) mice of similar age. Additionally, when the h*AGPAT2* expression is turned off by removing doxycycline (dox) from the diet of the animals, AT is undetectable within eight weeks in the mice.[16]

A primary goal of the present study was to determine whether regulated AT regeneration starting embryonically in dox-fed Tg-$^{AT\text{-}hA2}$;m$A2^{-/-}$ mice could result in the amelioration of hepatic steatosis and other metabolic derangements compared to that in chow-fed Tg-$^{AT\text{-}hA2}$;m$A2^{-/-}$ mice. Additionally, the study aimed to determine the normalization of metabolic derangements (i.e., hepatic steatosis and plasma glucose and insulin levels) in dox-fed Tg-$^{AT\text{-}hA2}$;m$A2^{-/-}$ mice, compared to those in chow-fed WT Tg-$^{AT\text{-}hA2}$;m$A2^{+/+}$ mice. Although the design of this study did not specifically address sex differences in the measured metabolic parameters, we highlighted the role of sex differences in the Results section. We report that upon AT regeneration, several metabolic features associated with lipodystrophy, including hepatic steatosis and insulin resistance (IR), show signs of improvement.

RESULTS

Construction of the Tg-$^{AT\text{-}hA2}$;m$A2^{-/-}$ mouse model

The generation and initial characterization of transgenic mice is described in our recently published article.[16] Briefly, for AT-specific re-expression of h*AGPAT2* in mice, we required generation and multiple crossing of three mouse lines: (1) a mouse strain expressing hAGPAT2 driven by the TRE-tight/PminCMV promoter system (refer to our previous study[16] for detailed experimental generation and characterization of mice); (2) a mouse strain expressing rtTA driven by an adiponectin promoter;[18] and (3) an *Agpat2*$^{+/-}$ mouse strain.[9] Our mating strategy and process of generating experimental mice are demonstrated in Figure S1D. The transgenic line we generated (Tg-$^{AT\text{-}hA2}$;m$A2^{-/-}$) is on a mixed genetic background of ~89% C57BL/6NTac and ~11% 129S6/SvEvTac. Likewise, the WT (B6129F1, abbreviated B6/129) mice used to ascertain the effect of dox diet were also on a mixed genetic background (~50% C57BL/6NTac and ~50% 129S6/SvEvTac).[17] The data for the chow-fed Tg-$^{AT\text{-}hA2}$;m$A2^{+/+}$ mice were the same as in our previous report,[16,17] as the experiments for all three studies were conducted concurrently. The mouse strain used in this study (Tg-h*AGPAT2, Adipo*-rtTA, m*Agpat2*$^{-/-}$) is hereafter referred to as Tg-$^{AT\text{-}hA2}$;m$A2^{-/-}$.This nomenclature/abbreviation denotes transgenic mice expressing h*AGPAT2* in a WT genetic background.

Feeding dox-containing diet to B6/129 mice did not change body weight or glucose tolerance

To measure whether the dox-containing diet will affect the experimental mice for the metabolic features, we tested B6/129 mice, a genetically unaltered strain (of mixed genetic background) routinely used as a control. We found no difference in animal body weights upon feeding dox-containing diet for 12 weeks or in glucose tolerance. This suggests that the dox diet fed for the duration of experiment does not have any confounding effect on the outcome of the current study. This observation is provided as supplemental data (Figure S2) and was recently published in the same journal.[17]

Regeneration of adipose tissue in dox-fed Tg-$^{AT\text{-}hA2}$;m$A2^{-/-}$ mice begins to ameliorate features of hepatic steatosis by 12 weeks of age and continues until 24 weeks

As previously reported,[9] *Agpat2*$^{-/-}$ mice on a chow diet usually have lower body weight in both sexes than WT mice, mostly because of the loss of AT. Groups of chow-fed Tg-$^{AT\text{-}hA2}$;m$A2^{+/+}$ (WT) mice, and both chow- and dox-fed Tg-$^{AT\text{-}hA2}$;m$A2^{-/-}$ mice of both sexes were weighed weekly starting at four weeks (once the genotyping was completed) until 12 weeks (Figures S3A and S3B). The Tg-$^{AT\text{-}hA2}$;m$A2^{-/-}$ mice of both sexes gained body weight when kept on dox food for 12 weeks (which allowed re-expression of h*AGPAT2* and regeneration of AT); in fact, they exhibited a slight weight gain compared to the WT mice on a chow diet (Figures 1A and 1I). The livers of chow-fed Tg-$^{AT\text{-}hA2}$;m$A2^{-/-}$ mice weighed more than those of the chow-fed WT mice, consistent with the anticipated hepatic steatosis. Moreover, the increase in liver weight was more pronounced in females than in males. This suggests that there is a sex-specific component to the metabolic complications of lipodystrophy in Tg-$^{AT\text{-}hA2}$;m$A2^{-/-}$ mice, although a specific cause of this disparity remains unknown. Regeneration of AT in dox-fed Tg-$^{AT\text{-}hA2}$;m$A2^{-/-}$ mice resulted in a decrease in liver weight compared to that in chow-fed Tg-$^{AT\text{-}hA2}$;m$A2^{-/-}$ mice (Figures 1B and 1J). Quantitatively, this reduction in liver weight is 19% in males and 59% in females at 12 weeks of age compared to that in chow-fed Tg-$^{AT\text{-}hA2}$;m$A2^{-/-}$ mice, reaching a statistical significance only in female mice ($p < 0.0001$). Because the chow-fed Tg-$^{AT\text{-}hA2}$;m$A2^{-/-}$ mice demonstrated lower body weights than the dox-fed Tg-$^{AT\text{-}hA2}$;m$A2^{-/-}$ mice, the ratio of liver weight to body weight showed a marked decrease compared to that in chow-fed Tg-$^{AT\text{-}hA2}$;m$A2^{-/-}$ mice in both sexes (55% in males, 68% in females) (Figures 1C and 1K). The ratios of liver/body weight of dox-fed Tg-$^{AT\text{-}hA2}$;m$A2^{-/-}$ mice decreased but remained above those of the chow-fed WT and only reached significance in females ($p = 0.002$). In fact, the liver weight in dox-fed Tg-$^{AT\text{-}hA2}$;m$A2^{-/-}$ mice was comparable to that of the WT mice maintained on a chow diet. We then measured the liver TAG levels, which showed a reduction in both sexes; however, this decrease only reached statistical significance in female mice ($p < 0.0001$; Figures 1D and 1L). The decrease in liver steatosis, or reduced fatty liver appearance, compared to that in the chow-fed mice can be noticed visually (Figures 1E–1G and 1M–1O). The decrease in the liver weight in dox-fed Tg-$^{AT\text{-}hA2}$;m$A2^{-/-}$ mice compared to that of chow-fed Tg-$^{AT\text{-}hA2}$;m$A2^{-/-}$ mice was found to be larger in females than in males. In female dox-fed Tg-$^{AT\text{-}hA2}$;m$A2^{-/-}$ mice, this could be attributed to increased regeneration of AT compared to males,[16] thereby correlating with how well the liver weight and TAG content decrease in female dox-fed Tg-$^{AT\text{-}hA2}$;m$A2^{-/-}$ mice. However, the underlying reason for the greater AT regeneration in female mice than in males remains unknown. Additionally, the plasma aspartate aminotransferase (AST) level, indicative of liver dysfunction, experienced a notable reduction to the extent that the AST levels in dox-fed Tg-$^{AT\text{-}hA2}$;m$A2^{-/-}$ mice became comparable to those in WT mice (Figures 1H and 1P). This suggests that the regenerated AT is physiologically functional and supports the fact that AT helps regulate liver fat.

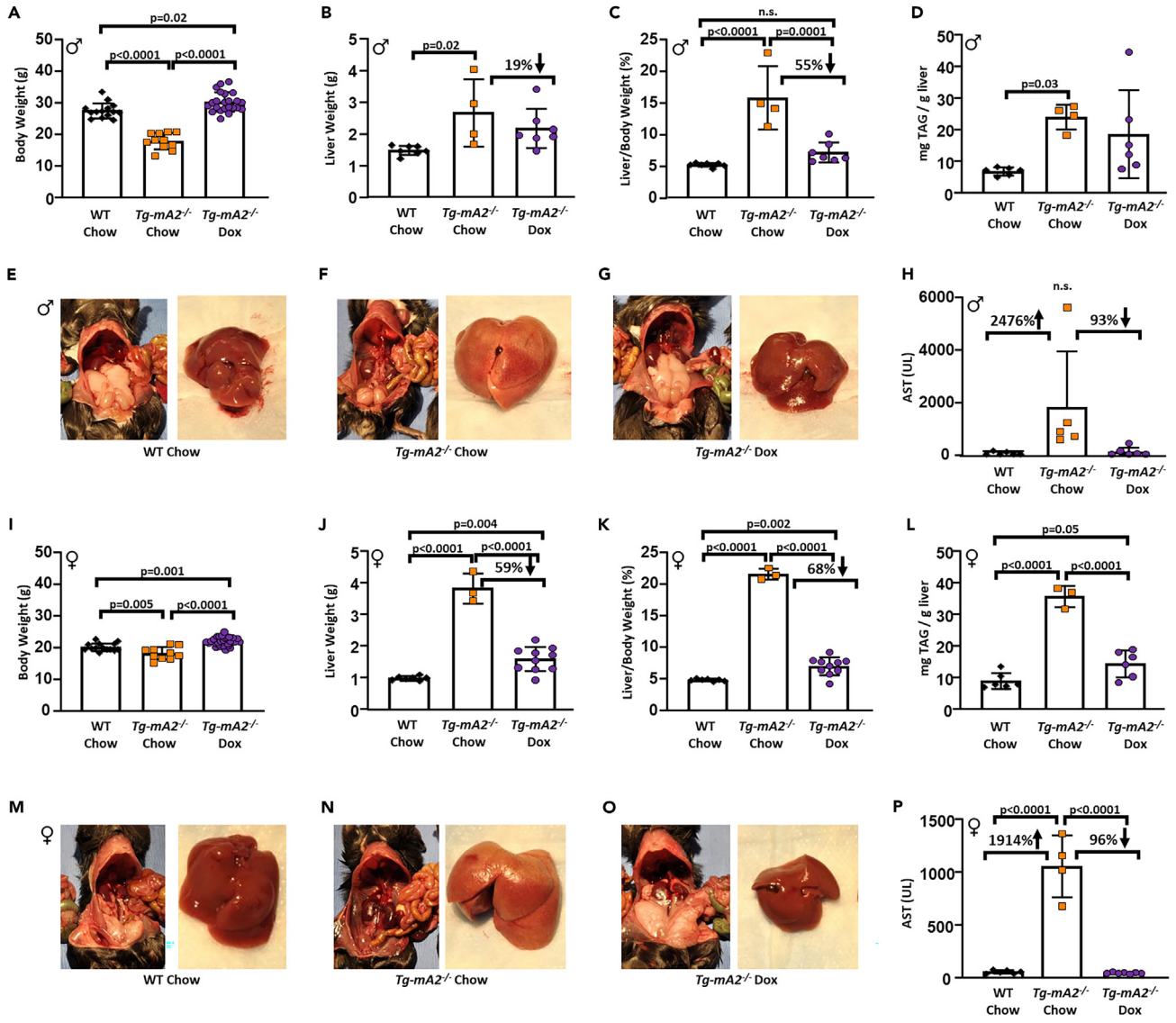

Figure 1. Decreased hepatic steatosis in 12 weeks dox-fed Tg-$^{AT\text{-}hA2}$;m$A2^{-/-}$ mice

(A and I) The body weight of (A) male and (I) female 12-week mice.

(B and J) The liver weight of (B) male and (J) female 12-week mice.

(C and K) the ratio of liver weight/body weight in (C) male and (K) female 12-week mice.

(D and L) The liver triacylglycerol (TAG) begins to decrease in both (D) male and (L) female dox-fed Tg-$^{AT\text{-}hA2}$;m$A2^{-/-}$ mice at 12 weeks compared to that in chow-fed Tg-$^{AT\text{-}hA2}$;m$A2^{-/-}$ mice.

(E–G) Visual images of adipose tissue (AT) *in situ* and liver excised at 12 weeks in (E) chow-fed WT, (F) chow-fed Tg-$^{AT\text{-}hA2}$;m$A2^{-/-}$, and (G) dox-fed Tg-$^{AT\text{-}hA2}$;m$A2^{-/-}$ male mice.

(H and P) Plasma aspartate aminotransferase (AST) levels decrease substantially in (H) male and (P) female dox-fed Tg-$^{AT\text{-}hA2}$;m$A2^{-/-}$ mice compared to that in chow-fed Tg-$^{AT\text{-}hA2}$;m$A2^{-/-}$ mice.

(M–O) Visual images of AT *in situ* and liver excised at 12 weeks in (M) chow-fed WT, (N) chow-fed Tg-$^{AT\text{-}hA2}$;m$A2^{-/-}$, and (O) dox-fed Tg-$^{AT\text{-}hA2}$;m$A2^{-/-}$ female mice. Data are represented as mean ± SD. Individual data points are shown within the bar. n = 3–28. p values were determined by one-way ANOVA. n.s., not significant. WT: Tg-$^{AT\text{-}hA2}$;m$A2^{+/+}$. Tg-$^{AT\text{-}hA2}$;m$A2^{-/-}$ abbreviated to **Tg-m$A2^{-/-}$**. See also Figure S4.

Regeneration of AT resulted in partial amelioration of hepatic steatosis in 12-week-old mice; therefore, we followed the mice for an additional 12 weeks to determine if the hepatic steatosis continued to improve. Groups of WT and Tg-$^{AT\text{-}hA2}$;m$A2^{-/-}$ mice, both chow- and dox-fed, of both sexes were weighed at 24 weeks of age (Figures S4A and S4I). Interestingly, at 24 weeks, the body weight of dox-fed Tg-$^{AT\text{-}hA2}$;m$A2^{-/-}$ mice considerably increased compared to that of chow-fed Tg-$^{AT\text{-}hA2}$;m$A2^{-/-}$ mice, albeit only in male mice. At 24 weeks, the chow-fed Tg-$^{AT\text{-}hA2}$;m$A2^{-/-}$ mice livers continued to deteriorate in terms of hepatic steatosis, and their liver weight was markedly higher than that of chow-fed

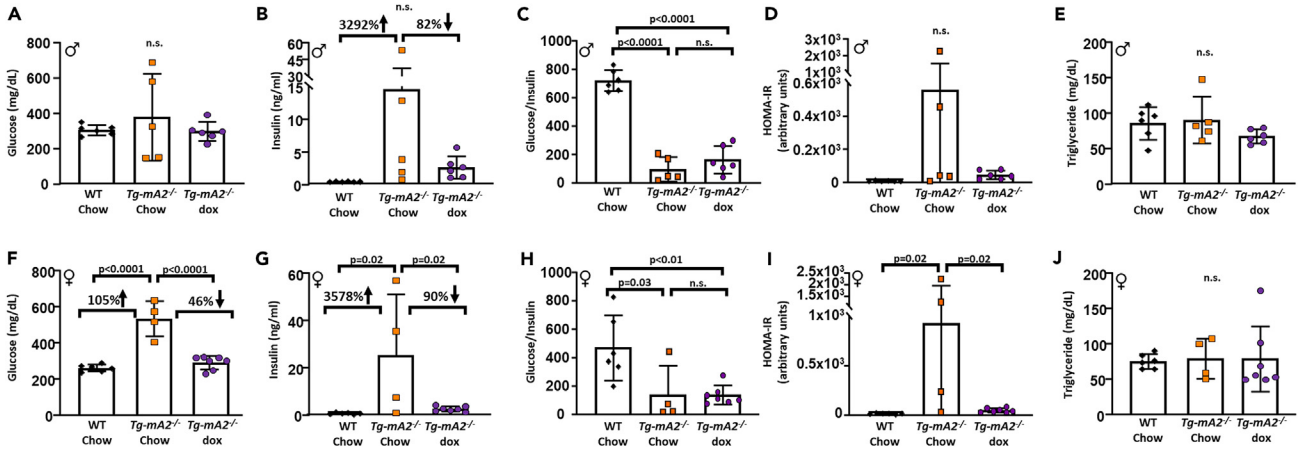

Figure 2. Plasma glucose, insulin, and triglyceride levels in 12 weeks non-fasting Tg-$^{AT\text{-}hA2}$;m$A2^{-/-}$ mice

(A and F) A decrease in non-fasting glucose levels is noted in (A) male and (F) female dox-fed Tg-$^{AT\text{-}hA2}$;m$A2^{-/-}$ mice compared to that in chow-fed Tg-$^{AT\text{-}hA2}$;m$A2^{-/-}$ mice, but only reaches statistical significance in females.

(B and G) (B) male and (G) female dox-fed Tg-$^{AT\text{-}hA2}$;m$A2^{-/-}$ mice also show decreases in insulin levels compared to that in chow-fed Tg-$^{AT\text{-}hA2}$;m$A2^{-/-}$ mice but reaches statistical significance only in female mice.

(C and H) When insulin resistance (IR) is determined as a ratio of glucose/insulin, it appears that both (C) male and (H) female dox-fed Tg-$^{AT\text{-}hA2}$;m$A2^{-/-}$ mice are as insulin resistant as the chow-fed Tg-$^{AT\text{-}hA2}$;m$A2^{-/-}$ mice when compared to that of the chow-fed wild type (WT) mice.

(D and I) IR as measured by a homeostatic model assessment of insulin resistance (HOMA-IR) in (D) male and (I) female mice. A greater value for HOMA-IR indicates a greater degree of IR, which can be seen in the chow-fed Tg-$^{AT\text{-}hA2}$;m$A2^{-/-}$ mice.

(E and J) There is no change in plasma triglycerides of either (E) males or (J) females. Data are represented as mean ± SD. Individual data points are shown within the bar. $n = 4–7$. p values are determined by one-way ANOVA. n.s., not significant. WT: Tg-$^{AT\text{-}hA2}$;m$A2^{+/+}$. Tg-$^{AT\text{-}hA2}$;m$A2^{-/-}$ abbreviated to Tg-m$A2^{-/-}$. See also Figure S5.

WT and dox-fed Tg-$^{AT\text{-}hA2}$;m$A2^{-/-}$ mice of both sexes (Figures S4B and S4J). Liver deterioration was even more apparent when expressed as a percentage of body weight (Figures S4C and S4K). At 12 weeks, the livers of chow-fed Tg-$^{AT\text{-}hA2}$;m$A2^{-/-}$ mice comprised 15% and 23% of the total body weight in male and female mice, respectively (Figures 1C and 1K). At 24 weeks, the liver percent of body weight increased to 20% of the total body weight in both male and female mice (Figures S4C and S4K). However, in dox-fed Tg-$^{AT\text{-}hA2}$;m$A2^{-/-}$ mice, the liver weight remained around 7% of the total body weight in both males and females. This improvement in liver size can be visually observed in Figures S4E–S4G and M–O. As expected, the liver TAG level markedly increased in chow-fed Tg-$^{AT\text{-}hA2}$;m$A2^{-/-}$ mice compared to that in chow-fed WT mice (Figures S4D and S4L). The TAG levels in dox-fed Tg-$^{AT\text{-}hA2}$;m$A2^{-/-}$ mice began to normalize to the levels observed in chow-fed WT mice. However, it did not reach statistical significance in males because of an outlier. Furthermore, the AST levels of dox-fed Tg-$^{AT\text{-}hA2}$;m$A2^{-/-}$ mice also normalized, making them comparable to those observed in chow-fed WT mice (Figures S4H and S4P).

Non-fasting plasma glucose and insulin levels in dox-fed Tg-$^{AT\text{-}hA2}$;m$A2^{-/-}$ mice normalize almost to WT levels at both 12 and 24 weeks

Non-fasting plasma glucose levels showed an increase in chow-fed Tg-$^{AT\text{-}hA2}$;m$A2^{-/-}$ mice compared to those in chow-fed WT mice of both sexes but only reached statistical significance in female mice ($p < 0.0001$; Figures 2A and 2F). When the Tg-$^{AT\text{-}hA2}$;m$A2^{-/-}$ mice were fed dox, thereby regenerating AT, we observed a decrease in the non-fasting plasma glucose levels approaching chow-fed WT levels, indicating a normalization of plasma glucose. This is also reflected in a decrease in the plasma insulin levels in the dox-fed Tg-$^{AT\text{-}hA2}$;m$A2^{-/-}$ mice compared to those in chow-fed Tg-$^{AT\text{-}hA2}$;m$A2^{-/-}$ mice (82% decrease in males, 90% decrease in females) (Figures 2B and 2G). Moreover, we only observed a considerable decrease in females but not in males, although this was complicated by the large variation in plasma insulin levels between individual chow-fed Tg-$^{AT\text{-}hA2}$;m$A2^{-/-}$ mice of both sexes. We examined IR in non-fasting plasma from both sexes using the ratio of glucose/insulin (Figures 2C and 2H) and the homeostatic model assessment of insulin resistance (HOMA-IR) (Figures 2D and 2I), which showed that both chow- and dox-fed Tg-$^{AT\text{-}hA2}$;m$A2^{-/-}$ mice were extensively insulin-resistant compared to chow-fed WT mice. However, as expected, when comparing chow- and dox-fed Tg-$^{AT\text{-}hA2}$;m$A2^{-/-}$ mice, there was an increase in insulin sensitivity in the dox-fed Tg-$^{AT\text{-}hA2}$;m$A2^{-/-}$ mice, with a statistical significance observed only in females ($p = 0.02$). As we observed with the liver weight and TAG levels, dox-fed Tg-$^{AT\text{-}hA2}$;m$A2^{-/-}$ female mice had a better response to fasting plasma glucose and insulin levels than dox-fed Tg-$^{AT\text{-}hA2}$;m$A2^{-/-}$ male mice, thereby reflecting the greater regeneration of AT in females.

In these transgenic mice, we did not observe any significant variation in non-fasting plasma triglycerides between chow-fed WT mice, chow-fed Tg-$^{AT\text{-}hA2}$;m$A2^{-/-}$ mice, or dox-fed Tg-$^{AT\text{-}hA2}$;m$A2^{-/-}$ mice in either sex (Figures 2E and 2J). This is contrary to our previous observations that *Agpat2*$^{-/-}$ mice exhibited increased plasma triglycerides.[9] This could be because of differences in the genetic background of the Tg-$^{AT\text{-}hA2}$;m$A2^{-/-}$ mice due to of the additional crossing needed to generate the transgenic line, which may have affected the triglyceride metabolism.

Plasma glucose levels in 24-week-old males were no different among the three groups studied; however, the glucose levels did decrease significantly (45% decrease) in female dox-fed Tg-$^{AT\text{-}hA2}$;m$A2^{-/-}$ mice compared to those in chow-fed Tg-$^{AT\text{-}hA2}$;m$A2^{-/-}$ mice (Figures S5A and S5E). The plasma insulin levels also considerably decreased in dox-fed Tg-$^{AT\text{-}hA2}$;m$A2^{-/-}$ mice compared to those in chow-fed Tg-$^{AT\text{-}hA2}$;m$A2^{-/-}$ mice of both sexes, with the levels nearing those of chow-fed WT mice (males—79%, females—89% decrease) (Figures S5B and S5F). We examined IR in non-fasting plasma for both sexes using the ratio of glucose/insulin and HOMA-IR (Figures S5C–S5D, S5H, and S5I). Chow-fed Tg-$^{AT\text{-}hA2}$;m$A2^{-/-}$ mice were considerably more insulin-resistant than chow-fed WT mice. Dox-fed Tg-$^{AT\text{-}hA2}$;m$A2^{-/-}$ mice also appeared to remain insulin-resistant, although there was a slight improvement in IR in female dox-fed Tg-$^{AT\text{-}hA2}$;m$A2^{-/-}$ mice compared to that in chow-fed Tg-$^{AT\text{-}hA2}$;m$A2^{-/-}$ mice, albeit not reaching statistical significance.

As observed for the 12-week plasma triglyceride levels, there was no significant difference between the groups studied at 24 weeks, except for a decrease (38% decrease) in female dox-fed Tg-$^{AT\text{-}hA2}$;m$A2^{-/-}$ mice compared to in chow-fed Tg-$^{AT\text{-}hA2}$;m$A2^{-/-}$ mice (Figures S5D and S5H). Overall, as more AT was regenerated over time (24 weeks), hepatic steatosis in dox-fed Tg-$^{AT\text{-}hA2}$;m$A2^{-/-}$ mice continued to improve; however, it did not return to levels similar to those of chow-fed WT mice.

Fasting chow- and dox-fed Tg-$^{AT\text{-}hA2}$;m$A2^{-/-}$ mice have similar oral glucose tolerance regardless of the absence or presence of AT at 12 weeks

There is a consensus that measurements of plasma glucose and insulin levels are sufficient to calculate IR, and various methods exist to calculate and interpret the ratios.[19] We have observed, in non-fasting chow-fed Tg-$^{AT\text{-}hA2}$;m$A2^{-/-}$ mice, that the plasma insulin levels were very high, which decreased upon regeneration of AT. This prompted us to measure the glucose tolerance of these mice using the oral glucose tolerance test (OGTT). We tested 12-week-old mice of both sexes that were fasted for 6 h. Figures 3A and 3G demonstrates the tail vein glucose measurements for 0–180 min after a bolus of gavaged glucose. In this experiment, chow-fed WT and chow-fed Tg-$^{AT\text{-}hA2}$;m$A2^{-/-}$ mice were comparable in terms of glucose tolerance, which was also reflected in the measurement of the area under the curve (AUC) (Figures 3B and 3H); however, we observed a wide variation between mice in the glucose tolerance in the dox-fed Tg-$^{AT\text{-}hA2}$;m$A2^{-/-}$ group. A few of the mice seemed to be more glucose intolerant, while others were not, as observed in the AUC. While the glucose levels seemed to be similar in WT and chow-fed Tg-$^{AT\text{-}hA2}$;m$A2^{-/-}$ mice, dox-fed Tg-$^{AT\text{-}hA2}$;m$A2^{-/-}$ mice had higher plasma glucose levels at 30 and 60 min than those of the other groups. Furthermore, the plasma glucose levels in dox-fed Tg-$^{AT\text{-}hA2}$;m$A2^{-/-}$ mice did not return to the baseline and were still not statistically significant. Fasting plasma glucose and insulin are a good measure of IR, which can be calculated by a simple ratio of glucose/insulin at time 0 (T_0) or using HOMA-IR. While there was no significant difference in fasting plasma glucose levels among the three groups studied (Figures 3C and 3I), the fasting insulin levels in dox-fed Tg-$^{AT\text{-}hA2}$;m$A2^{-/-}$ mice returned to levels seen in chow-fed WT mice (Figures 3D and 3J). The T_0 glucose/insulin ratio showed that chow-fed Tg-$^{AT\text{-}hA2}$;m$A2^{-/-}$ mice had considerably increased IR compared to chow-fed WT mice for both sexes (Figures 3E and 3K). When IR was measured using the HOMA-IR method, only the female chow-fed Tg-$^{AT\text{-}hA2}$;m$A2^{-/-}$ mice had a significant increase in IR compared to chow-fed WT mice ($p = 0.004$; Figures 3F and 3L). In the dox-fed mice, compared to that in the chow-fed Tg-$^{AT\text{-}hA2}$;m$A2^{-/-}$ mice, IR began to improve but only reached statistical significance ($p = 0.01$) in females using either method of calculation of IR. However, dox-fed Tg-$^{AT\text{-}hA2}$;m$A2^{-/-}$ mice did not reach a comparable level of insulin sensitivity as that of chow-fed WT mice. The reason underlying the fact that female mice were more insulin-sensitive compared to male mice in this dox-fed Tg-$^{AT\text{-}hA2}$;m$A2^{-/-}$ line was unclear.

With partial amelioration of hepatic steatosis at 12 weeks, we would expect dox-fed Tg-$^{AT\text{-}hA2}$;m$A2^{-/-}$ mice to be more glucose tolerant than chow-fed Tg-$^{AT\text{-}hA2}$;m$A2^{-/-}$ mice at 24 weeks; therefore, we repeated the OGTT at 24 weeks. After 6 h fasting, at time 0, the tail vein glucose levels were similar among the three groups studied. The male and female mice exhibited differences in their glucose tolerance (Figures S6A and S6F). However, the AUC shown in Figures S6B and S6G demonstrated no statistical significance between the groups studied. However, fasting plasma glucose was more remarkable. As observed during 12 weeks, 24-week dox-fed Tg-$^{AT\text{-}hA2}$;m$A2^{-/-}$ mice achieved similar fasting glucose plasma levels to those of chow-fed WT mice (Figures S6C and S6H). Here, chow-fed Tg-$^{AT\text{-}hA2}$;m$A2^{-/-}$ mice also showed remarkably elevated plasma insulin levels, although this did not reach statistical significance in male mice (Figures S6D and S6I). When compared to those of chow-fed Tg-$^{AT\text{-}hA2}$;m$A2^{-/-}$ mice, dox-fed Tg-$^{AT\text{-}hA2}$;m$A2^{-/-}$ mice had decreased plasma insulin levels for both sexes (Figures S6D and S6I), reaching statistical significance only in female mice. As expected, the T_0 glucose/insulin ratio demonstrated that chow-fed Tg-$^{AT\text{-}hA2}$;m$A2^{-/-}$ mice remained insulin-resistant (Figures S6E and S6J). Another observation of interest was that while fasting glucose levels were similar among the three groups studied, the insulin level decreased only in dox-fed Tg-$^{AT\text{-}hA2}$;m$A2^{-/-}$ mice but not in chow-fed Tg-$^{AT\text{-}hA2}$;m$A2^{-/-}$ mice. The Discussion section explores the existence of a correlation between plasma glucose and insulin levels.

Doxycycline-fed Tg-$^{AT\text{-}hA2}$;m$A2^{-/-}$ mice are as insulin sensitive as WT (Tg-$^{AT\text{-}hA2}$;m$A2^{+/+}$) mice based on insulin tolerance tests

To estimate insulin sensitivity, we used the insulin tolerance test (ITT), a widely used test employed for assessing IR, to measure the plasma glucose levels via tail vein in 3 h fasted dox-fed Tg-$^{AT\text{-}hA2}$;m$A2^{-/-}$ mice and compared these results to those of chow-fed WT mice. The insulin tolerance test (ITT) revealed that upon insulin administration, the plasma glucose levels showed no statistical differences between dox-fed Tg-$^{AT\text{-}hA2}$;m$A2^{-/-}$ mice and WT mice in both sexes (Figure S7). A good comparison would have been to compare these results between the chow-fed and dox-fed Tg-$^{AT\text{-}hA2}$;m$A2^{-/-}$ mice. Unfortunately, chow-fed *Agpat2*$^{-/-}$ mice had extremely high plasma insulin levels such that it precluded us from carrying out the ITT in these mice (in-house observation). Nevertheless, a comparison between dox-fed Tg-$^{AT\text{-}hA2}$;m$A2^{-/-}$ mice and WT mice showed that dox-fed Tg-$^{AT\text{-}hA2}$;m$A2^{-/-}$ mice became insulin-sensitive because of AT regeneration.

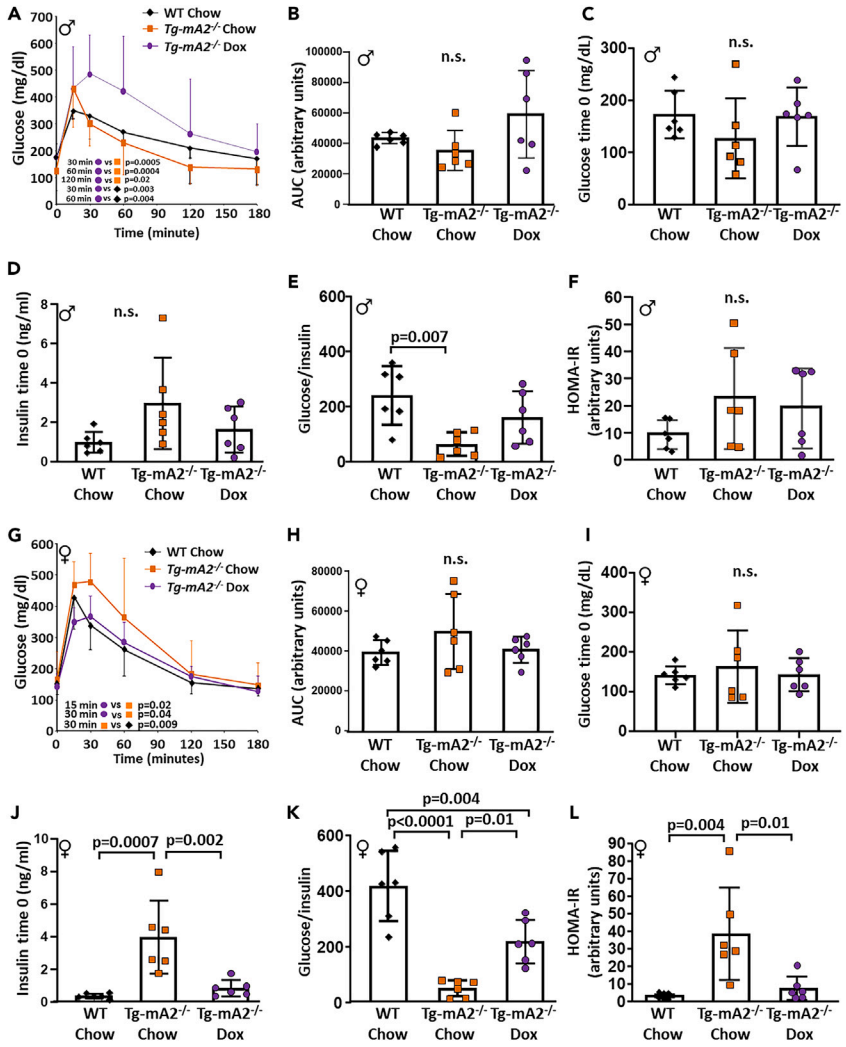

Figure 3. Oral glucose tolerance test (OGTT) in 12-week Tg-$^{AT\text{-}hA2}$;$mA2^{-/-}$ mice

(A and G) The glucose clearance in 12-week (A) male and (G) female dox- and chow-fed Tg-$^{AT\text{-}hA2}$;$mA2^{-/-}$ mice.

(B and H) The same data points are used to generate the area under the curve (AUC) to determine the total glucose clearance (time 0–180 min) in (B) male and (H) female mice. *p* values are determined using mixed model repeat measurements. We note no significant difference in the AUC between dox- or chow-fed Tg-$^{AT\text{-}hA2}$;$mA2^{-/-}$ mice.

(C and I) Fasting (6 h) plasma glucose in 12-week (C) male and (I) female mice.

(D and J) Fasting (6 h) plasma insulin in 12-week (D) male and (J) female. At time 0, insulin levels decrease in female mice only.

(E and K) A ratio of glucose/insulin at time 0 indicates that the (E) male and (K) female dox-fed Tg-$^{AT\text{-}hA2}$;$mA2^{-/-}$ mice have improved glucose tolerance.

(F and L) A measurement of insulin resistance (IR) using the homeostatic model assessment of insulin resistance (HOMA-IR) shows no change in IR in (F) male mice, but a significant decrease in IR (L) in female dox-fed Tg-$^{AT\text{-}hA2}$;$mA2^{-/-}$ mice compared to that in chow-fed Tg-$^{AT\text{-}hA2}$;$mA2^{-/-}$ mice. In fact, there is no significant difference in the IR of female dox-fed Tg-$^{AT\text{-}hA2}$;$mA2^{-/-}$ mice compared to that in chow-fed wild type (WT) mice, indicating that regeneration of adipose tissues brings IR back to WT levels in a fasting state. Data are represented as mean ± SD. Individual dots represent independent mice. Individual data points are shown within the bar. $n = 6$. *p* values are determined by one-way ANOVA. n.s., not significant. WT: Tg-$^{AT\text{-}hA2}$;$mA2^{+/+}$. Tg-$^{AT\text{-}hA2}$;$mA2^{-/-}$ abbreviated to Tg-$mA2^{-/-}$. See also Figure S6.

A decrease in hepatic steatosis also results in the decreased expression of key transcripts for fatty acid and TAG synthesis, insulin and insulin-like growth factor (*Igf*) signaling pathways, and glucose metabolism in dox-fed Tg-$^{AT\text{-}hA2}$;$mA2^{-/-}$ mice compared to those in chow-fed Tg-$^{AT\text{-}hA2}$;$mA2^{-/-}$ mice at 12 and 24 weeks

The canonical insulin signaling pathway is well described.[20] Insulin binds to the cell surface insulin receptors, which undergo autophosphorylation, recruiting insulin receptor substrates (IRS) 1 and 2. The phosphorylated IRS can then recruit phosphatidylinositol 3-kinase (PI3K) to the cell surface and phosphorylate phosphatidylinositol 4,5-bisphosphate (PIP2) to phosphatidylinositol (3,4,5)-trisphosphate (PIP3), which

Table 1. RT-qPCR measurements of key genes for *de novo* lipogenesis pathways, triacylglycerol (TAG) synthesis, fatty acid oxidation, insulin and insulin-like growth factor (*Igf*) pathways, and glucose metabolism in livers of 12 weeks chow-fed wild-type (WT) and chow- and doxycycline (dox)-fed Tg-$^{AT\text{-}hA2}$;*mA2*$^{-/-}$ mice

Sex	Male					Female				
Genotype	WT	Tg-*mA2*$^{-/-}$	Tg-*mA2*$^{-/-}$	Tg-*mA2*$^{-/-}$		WT	Tg-*mA2*$^{-/-}$	Tg-*mA2*$^{-/-}$	Tg-*mA2*$^{-/-}$	
Diet	Chow	Chow	Dox	Chow	Dox	Chow	Chow	Dox	Chow	Dox
Samples pooled (n)	6	4	6	4	6	6	3	6	3	6
Group comparison		A	B	C			A	B	C	
Gene										
Fatty acid and TAG synthesis										
Acly	1.00	1.76 ± 0.02	2.04 ± 0.14	1.00	1.16 ± 0.09	1.00	1.74 ± 0.22	2.05 ± 0.13	1.00	1.19 ± 0.23
Acc1	1.00	2.53 ± 0.17	2.20 ± 0.26	1.00	0.87 ± 0.04	1.00	2.93 ± 0.07	1.73 ± 0.13	1.00	0.59 ± 0.03
Fas	1.00	2.82 ± 0.07	1.77 ± 0.04	1.00	0.63 ± 0.03	1.00	2.31 ± 0.08	1.87 ± 0.04	1.00	0.81 ± 0.01
Elovl6	1.00	3.87 ± 0.27	3.28 ± 0.20	1.00	0.85 ± 0.01	1.00	2.64 ± 0.04	1.88 ± 0.01	1.00	0.71 ± 0.01
Scd1	1.00	2.06 ± 0.43	2.05 ± 0.44	1.00	1.00 ± 0.00	1.00	2.61 ± 0.36	1.09 ± 0.08	1.00	0.42 ± 0.03
Scd2	1.00	40.13 ± 3.97	2.64 ± 0.43	1.00	0.07 ± 0.00	1.00	62.39 ± 3.21	1.19 ± 0.06	1.00	0.02 ± 0.00
Gpat1	1.00	2.25 ± 0.07	2.22 ± 0.12	1.00	0.99 ± 0.02	1.00	2.76 ± 0.01	2.01 ± 0.07	1.00	0.73 ± 0.02
mAgpat2	1.00	0.00 ± 0.00[a]	0.00 ± 0.00[a]	1.00[a]	0.32 ± 0.09[a]	1.00	0.01 ± 0.00	0.00 ± 0.00[a]	1.00	0.04 ± 0.04[a]
Ppap2c	1.00	2.57 ± 0.32	0.96 ± 0.10	1.00	0.38 ± 0.01	1.00	3.45 ± 0.08	0.85 ± 0.01	1.00	0.25 ± 0.01
Lipin 3	1.00[a]	3.22 ± 0.02	0.93 ± 0.15	1.00	0.29 ± 0.04	1.00[a]	3.76 ± 0.05	1.34 ± 0.13[a]	1.00	0.36 ± 0.04[a]
Dgat2	1.00	0.76 ± 0.02	1.08 ± 0.12	1.00	1.42 ± 0.12	1.00	1.03 ± 0.03	1.37 ± 0.03	1.00	1.33 ± 0.06
Mogat1	1.00[a]	36.11 ± 5.35	34.34 ± 5.43	1.00	0.95 ± 0.01	1.00[a]	141.09 ± 12.87	39.88 ± 2.39	1.00	0.28 ± 0.01
Pparγ	1.00	2.34 ± 0.06	2.80 ± 0.03	1.00	1.20 ± 0.02	1.00	2.74 ± 0.25	1.58 ± 0.04	1.00	0.58 ± 0.04
Fatty acid oxidation										
Pparα	1.00	0.72 ± 0.10	1.12 ± 0.10	1.00	1.57 ± 0.08	1.00	0.90 ± 0.01	1.34 ± 0.00	1.00	1.48 ± 0.03
Ucp2	1.00	10.27 ± 0.52	1.82 ± 0.14	1.00	0.18 ± 0.00	1.00	6.99 ± 0.35	1.51 ± 0.15	1.00	0.22 ± 0.01
SREBP pathway										
Srebp-1a	1.00	1.05 ± 0.02	0.85 ± 0.07	1.00	0.81 ± 0.06	1.00	1.50 ± 0.08	1.34 ± 0.12	1.00	0.89 ± 0.03
Srebp-1c	1.00	0.71 ± 0.08	1.56 ± 0.12	1.00	2.19 ± 0.06	1.00	0.70 ± 0.07	2.19 ± 0.06	1.00	3.14 ± 0.24
Insig 1	1.00	0.70 ± 0.06	1.11 ± 0.12	1.00	1.58 ± 0.04	1.00	0.62 ± 0.10	1.06 ± 0.12	1.00	1.72 ± 0.08
Insig 2	1.00	1.73 ± 0.07	1.94 ± 0.13	1.00	1.12 ± 0.03	1.00	1.64 ± 0.05	1.42 ± 0.06	1.00	0.86 ± 0.01
Scap	1.00	0.50 ± 0.06	0.70 ± 0.06	1.00	1.42 ± 0.04	1.00	0.56 ± 0.03	0.77 ± 0.03	1.00	1.38 ± 0.03
Insulin and IGF-1 signaling										
IR	1.00	0.83 ± 0.02	0.89 ± 0.04	1.00	1.07 ± 0.02	1.00	1.29 ± 0.03	1.05 ± 0.02	1.00	0.81 ± 0.03
Irs-1	1.00	0.74 ± 0.04	0.84 ± 0.04	1.00	1.15 ± 0.12	1.00	0.94 ± 0.09	1.12 ± 0.06	1.00	1.19 ± 0.06
Irs-2	1.00	0.52 ± 0.03	0.70 ± 0.04	1.00	1.36 ± 0.01	1.00	0.61 ± 0.07	0.62 ± 0.03	1.00	1.02 ± 0.06
Igf-1 R	1.00[a]	2.53 ± 0.75	1.03 ± 0.14	1.00	0.42 ± 0.07[a]	1.00[a]	3.58 ± 0.02	1.39 ± 0.01[a]	1.00	0.39 ± 0.00[a]
Igf-1	1.00	0.26 ± 0.01	0.87 ± 0.06	1.00	3.41 ± 0.11	1.00	0.18 ± 0.01	1.14 ± 0.04	1.00	6.33 ± 0.13
Igf-bp	1.00	8.46 ± 0.71	1.43 ± 0.18	1.00	0.17 ± 0.01	1.00	6.01 ± 0.31	1.32 ± 0.02	1.00	0.22 ± 0.01
Glucose metabolism										
Chrebp	1.00	0.57 ± 0.02	0.90 ± 0.08	1.00	1.59 ± 0.08	1.00	0.78 ± 0.02	1.06 ± 0.04	1.00	1.34 ± 0.00
Pepck	1.00	0.64 ± 0.04	0.77 ± 0.04	1.00	1.21 ± 0.02	1.00	0.65 ± 0.02	0.92 ± 0.06	1.00	1.41 ± 0.04

(*Continued on next page*)

Table 1. *Continued*

Sex	Male					Female				
Genotype	WT	Tg-m*A2*$^{-/-}$	Tg-m*A2*$^{-/-}$	Tg-m*A2*$^{-/-}$		WT	Tg-m*A2*$^{-/-}$	Tg-m*A2*$^{-/-}$	Tg-m*A2*$^{-/-}$	
Diet	Chow	Chow	Dox	Chow	Dox	Chow	Chow	Dox	Chow	Dox
Samples pooled (n)	6	4	6	4	6	6	3	6	3	6
Group comparison		A	B	C			A	B	C	
Gene										
G-6-Pase	1.00	1.13 ± 0.08	1.15 ± 0.02	1.00	1.02 ± 0.06	1.00	1.75 ± 0.01	1.59 ± 0.07	1.00	0.91 ± 0.04
Pk	1.00	1.78 ± 0.05	1.21 ± 0.00	1.00	0.68 ± 0.02	1.00	2.22 ± 0.04	1.83 ± 0.14	1.00	0.82 ± 0.05

Shown are comparisons of the expression of transcripts (mRNA) between the groups as follows; A—chow-fed WT compared to chow-fed Tg-AT-hA2;m*A2*$^{-/-}$ mice, B—chow-fed WT compared to dox-fed Tg-AT-hA2;m*A2*$^{-/-}$ mice, C—chow-fed Tg-AT-hA2;m*A2*$^{-/-}$ mice compared to dox-fed Tg-AT-hA2;m*A2*$^{-/-}$ mice. An equal quantity of total RNA is pooled from each mouse (shown in the table), quantified twice in duplicate, and presented as mean ± SD. Data are shown compared to chow-fed WT mice = 1 (group A and B) and chow-fed Tg-AT-hA2;m*A2*$^{-/-}$ mice = 1 (group C).

[a]Indicates a raw C_t value >30. Wherever the raw C_t value >30, we consider the fold change as approximate. For the human transgene *hAGPAT2*, the raw C_t values are as follows: in males, WT C_t = 31.26, chow-fed Tg-AT-hA2;m*A2*$^{-/-}$ C_t = 29.47, dox-fed Tg-AT-hA2;m*A2*$^{-/-}$ C_t = 30.38; C_t values are similar for females. WT: Tg-AT-hA2;m*A2*$^{+/+}$. Tg-AT-hA2;m*A2*$^{-/-}$ is abbreviated to Tg-m*A2*$^{-/-}$.

recruits pyruvate dehydrogenase kinase isozyme 1 (PDK1) and RAC-beta serine/threonine-protein kinase (AKT2) that are then phosphorylated. AKT2 activates mechanistic target of rapamycin kinase (mTOR), resulting in the phosphorylation of transcription factor forkhead box O1 (FOXO1). We measured several of these key insulin signaling elements at both the transcript and protein levels.

Here, we compared the expression of transcripts (mRNA) between the groups as follows: A—chow-fed WT compared to chow-fed Tg-$^{AT\text{-}hA2}$;m*A2*$^{-/-}$ mice, B—chow-fed WT compared to dox-fed Tg-$^{AT\text{-}hA2}$;m*A2*$^{-/-}$ mice, and C—chow-fed Tg-$^{AT\text{-}hA2}$;m*A2*$^{-/-}$ mice compared to dox-fed Tg-$^{AT\text{-}hA2}$;m*A2*$^{-/-}$ mice (Table 1). In general, a comparison between chow-fed WT and Tg-$^{AT\text{-}hA2}$;m*A2*$^{-/-}$ mice for both sexes (Table 1, group A) showed that the mRNA for fatty acid and TAG synthesis, insulin and insulin-like growth factor (*Igf*) signaling, and glucose metabolism pathways were all activated, except for sterol regulatory element-binding protein 1 (*Srebp-1c*), as we have previously reported[9], which regulated these pathways. We also observed that while the insulin signaling pathway was suppressed, the IGF pathway was increased, specifically insulin-like growth factor binding protein (IGF-BP). The activation of these pathways is similar to that reported in *Agpat2*$^{-/-}$ mice.[9] We are reporting this new murine model with a slightly varied genetic background expressing the h*AGPAT2* transgene. While the transgene was not activated (which required dox) and should not have been present in the liver, a small increase was noted, which could account for leakiness of transgene expression in the liver.

The decreased TAG levels in the livers of dox-fed Tg-$^{AT\text{-}hA2}$;m*A2*$^{-/-}$ mice was also reflected by the decrease in the expression of key transcripts for fatty acid and TAG synthesis genes. In general, the expression was decreased in dox-fed Tg-$^{AT\text{-}hA2}$;m*A2*$^{-/-}$ mice compared to in chow-fed Tg-$^{AT\text{-}hA2}$;m*A2*$^{-/-}$ mice (Table 1, group C), although the levels were still slightly higher compared to that in chow-fed WT mice (Table 1, group B). Compared to chow-fed Tg-$^{AT\text{-}hA2}$;m*A2*$^{-/-}$ mice as fold change = 1, the most marked decrease in the dox-fed Tg-$^{AT\text{-}hA2}$;m*A2*$^{-/-}$ mice (Table 1, group C) was in the expression of *Scd2* (male—0.07, female—0.02-fold), the phosphorylase *Ppap2c* (male—0.38, female—0.25-fold), and *Lipin 3* (male—0.29, female—0.36-fold), in both sexes. While we previously noted *Mogat1* being upregulated in livers of ***Agpat2***$^{-/-}$ mice,[9] we observed a sex-specific down-regulation of *Mogat1* in female Tg-$^{AT\text{-}hA2}$;m*A2*$^{-/-}$ mice but not in males (males—0.95, females—0.28-fold) upon AT regeneration.

For transcripts related to fatty acid oxidation, *Pparα* did not change, but *Ucp2* decreased several folds in dox-fed Tg-$^{AT\text{-}hA2}$;m*A2*$^{-/-}$ mice of both sexes compared to that in chow-fed Tg-$^{AT\text{-}hA2}$;m*A2*$^{-/-}$ mice. We previously reported that *Srebp-1c* was not upregulated in the livers of ***Agpat2***$^{-/-}$ mice.[9] In this study, we noted a slight increase in *Srebp-1c* expression in dox-fed Tg-$^{AT\text{-}hA2}$;m*A2*$^{-/-}$ mice of both sexes compared to that in chow-fed WT mice (male—1.56-fold, female—2.19-fold). The increase in *Srebp-1c* expression could be more appreciated when dox-fed Tg-$^{AT\text{-}hA2}$;m*A2*$^{-/-}$ mice were compared to chow-fed Tg-$^{AT\text{-}hA2}$;m*A2*$^{-/-}$ mice (male—2.19-fold, female—3.14-fold).

Despite the amelioration in plasma insulin levels and hepatic steatosis in dox-fed Tg$^{-AT\text{-}hA2}$;mA2$^{-/-}$, the key insulin signaling transcripts did not change in either chow or dox-fed Tg-$^{AT\text{-}hA2}$;m*A2*$^{-/-}$ mice of both sexes compared to that of chow-fed WT mice (Table 1, groups A and B), although we observed changes in the IGF signaling pathway. The expression of *Igf-r* (insulin-like growth factor-receptor) was not detected in chow-fed WT mice or in dox-fed Tg-$^{AT\text{-}hA2}$;m*A2*$^{-/-}$ mice of both sexes, but it was approximately 2- to 3-fold upregulated in chow-fed Tg-$^{AT\text{-}hA2}$;m*A2*$^{-/-}$ mice. However, this fold change was approximate, as the chow-fed WT C_t >30. We observed a 3.8- to 5.5-fold decrease in the expression of the ligand for the *Igf-r Igf-1*, in chow-fed Tg-$^{AT\text{-}hA2}$;m*A2*$^{-/-}$ mice compared to that in chow-fed WT mice. However, the expression of *Igf-1* in dox-fed Tg-$^{AT\text{-}hA2}$;m*A2*$^{-/-}$ mice was normalized to WT levels of *Igf-1*. Additionally, *Igf-bp* was upregulated by 6- to 8-fold in the chow-fed Tg-$^{AT\text{-}hA2}$;m*A2*$^{-/-}$ mice compared to that in the chow-fed WT mice. Again, the expression of *Igf-bp* in dox-fed Tg-$^{AT\text{-}hA2}$;m*A2*$^{-/-}$ mice was normalized to WT levels. The regulation of the insulin and IGF signaling pathways were independently regulated in our murine model. We were expecting changes in the expression of *Chrebp* (carbohydrate response element binding protein) as carbohydrate metabolism is

regulated by *Chrebp*;[21] however, gene expression of transcripts for glucose metabolism (phosphoenolpyruvate carboxykinase (ATP) [*Pepck*], glucose-6-phosphatase [*G-6-pase*], and pyruvate kinase [*Pk*]) remained unaffected.

Collectively, a comparison of chow- to dox-fed Tg-$^{AT\text{-}hA2}$;m$A2^{-/-}$ mice (Table 1, group C) showed a marked decrease in the expression of genes related to fatty acid and TAG synthesis in the livers of female mice but not in male mice. In female dox-fed Tg-$^{AT\text{-}hA2}$;m$A2^{-/-}$ mice, fatty acid and TAG synthesis gene expression normalized to near chow-fed WT levels (Table 1, group B). In males, many of the genes that were upregulated in chow-fed Tg-$^{AT\text{-}hA2}$;m$A2^{-/-}$ mice remained upregulated compared to those in chow-fed WT levels in dox-fed Tg-$^{AT\text{-}hA2}$;m$A2^{-/-}$ mice. The expression of several of the genes for insulin signaling in both male and female dox-fed Tg-$^{AT\text{-}hA2}$;m$A2^{-/-}$ mice also returned to levels of chow-fed WT mice. This was consistent with the response in female dox-fed Tg-$^{AT\text{-}hA2}$;m$A2^{-/-}$ mice with regards to AT regeneration and amelioration of hepatic steatosis.

In general, the expression of key genes either further increased in chow-fed Tg-$^{AT\text{-}hA2}$;m$A2^{-/-}$ mice or decreased in dox-fed Tg-$^{AT\text{-}hA2}$;m$A2^{-/-}$ mice when compared to those in WT mice at 24 weeks (Table S1, groups A and B). This was also true when chow-fed Tg-$^{AT\text{-}hA2}$;m$A2^{-/-}$ mice were compared to dox-fed Tg-$^{AT\text{-}hA2}$;m$A2^{-/-}$ mice (Table S1, group C). We also noted that while the expression of *Mogat1* in 12-week male dox-fed Tg-$^{AT\text{-}hA2}$;m$A2^{-/-}$ mice did not decrease compared to that in chow-fed Tg-$^{AT\text{-}hA2}$;m$A2^{-/-}$ mice (0.95-fold), it decreased in males (0.39-fold) at 24 weeks.

Measurements of liver proteins and phosphopeptides related to insulin signaling and glucose metabolism in the livers of Tg-$^{AT\text{-}hA2}$;m$A2^{-/-}$ mice using tandem mass tag-mass spectrometry

In addition to canonical insulin signaling, we also measured a few of the non-canonical insulin signaling proteins, including IGF, which also binds to and activates the insulin receptors.[22] We adopted the tandem mass tag-mass spectrometry (TMT-MS) approach to circumvent the use of several antibodies for both native proteins and their phosphorylated forms as, on occasion, the specificity of these antibodies are not highly curated. We also adopted a phosphoprotein/phosphopeptide detection and quantification approach, which requires additional steps in processing and identification, since mRNA cannot ascertain post-translationally modified proteins. We measured the liver proteins in 12-week-old chow-fed WT mice and chow- and dox-fed Tg-$^{AT\text{-}hA2}$;m$A2^{-/-}$ mice of both sexes. Table 2 shows the proteins of the insulin signaling pathways, and Table 3 shows the identified phosphorylated peptides of the respective proteins. The comparison of the protein expression between groups was the same as that for the mRNA (Table 1). In group A, for both sexes, there was a modest but consistent (~1.5- to 2.5-fold) increase in protein detection for the insulin signaling pathway in chow-fed Tg-$^{AT\text{-}hA2}$;m$A2^{-/-}$ mice compared to in chow-fed WT mice. As expected, chow-fed Tg-$^{AT\text{-}hA2}$;m$A2^{-/-}$ mice were IR, and the livers of these mice tried to synthesize proteins to overcome the resistance to insulin signaling. Upon comparing chow-fed WT versus dox-fed Tg-$^{AT\text{-}hA2}$;m$A2^{-/-}$ mice in group B, we observed that the proteins of the insulin signaling pathway began to normalize in both sexes. These observations showed that the liver insulin signaling in dox-fed Tg-$^{AT\text{-}hA2}$;m$A2^{-/-}$ mice was almost normalized to that of the chow-fed WT levels, confirming a regulation of insulin signaling because of AT regeneration in dox-fed Tg-$^{AT\text{-}hA2}$;m$A2^{-/-}$ mice. IGF1 was 2- to 5-fold upregulated in chow-fed Tg-$^{AT\text{-}hA2}$;m$A2^{-/-}$ mice compared to in chow-fed WT mice for both sexes (Table 2, group A). When hAGPAT2 was expressed in AT, the levels in dox-fed Tg-$^{AT\text{-}hA2}$;m$A2^{-/-}$ mice normalized to the levels in chow-fed WT mice (Table 2, group B). The expression of key proteins for glucose metabolism[21] were also upregulated; as expected, CHREBP (MLXIPL) expression was markedly upregulated approximately 3-fold in chow-fed Tg-$^{AT\text{-}hA2}$;m$A2^{-/-}$ mice of both sexes compared to in chow-fed WT mice (Table 2, group A). Protein levels began to normalize to chow-fed WT levels upon feeding dox (re-expressing hAGPAT2 in AT) to Tg-$^{AT\text{-}hA2}$;m$A2^{-/-}$ mice (Table 2, group B). When compared to those of chow-fed Tg-$^{AT\text{-}hA2}$;m$A2^{-/-}$ mice, the protein levels in the dox-fed Tg-$^{AT\text{-}hA2}$;m$A2^{-/-}$ mice decreased (Table 2, group C). Insulin signaling could also be partly modulated by insulin-degrading enzyme (IDE).[23] We were intrigued by this protein, as it may elucidate the variations in male-female insulin signaling. Notably, we observed no difference in IDE protein levels in either sex.

In our phosphopeptide enrichment and detection assay, though we were unable to reliably measure all the key phosphoproteins/phosphopeptides, we detected some of them, including mTOR complex 1, AKT1/2, glycogen synthase kinase 3 alpha (GSK3), phosphoenolpyruvate carboxykinase 1 (PCK1), and CHREBP. We encountered a few technical challenges, including inadequate peptide generation because of the proteolytic cleavage protease employed. We detected a phosphopeptide that was identified both in AKT1 and AKT2, but we were unable to distinguish between the two isoforms (Table 3; Figure S8). Another example was PCK1. The phosphoprotein/phosphopeptide that was detected aligned to both the muscle and liver isoforms, where it was not possible to distinguish between the two proteins. Although we detected the forkhead box O3 (FOXO3) protein, we did not detect its phosphorylated form. The most abundant phosphopeptide among the proteins was detected for CHREBP. While we did not detect remarkable changes at the mRNA level, we noted a marked increase in the CHREBP phosphopeptides in chow-fed Tg-$^{AT\text{-}hA2}$;m$A2^{-/-}$ mice. This phosphorylation returned to WT levels in the dox-fed Tg-$^{AT\text{-}hA2}$;m$A2^{-/-}$ mice. CHREBP requires phosphorylation for its hepatic transcriptional activation of target genes. In addition, as expected, we did not detect the hAGAPT2 protein in the livers, as this was not expected to be expressed in the liver.

Measurement of food intake, water intake, respiratory exchange ratio, and energy regulation via indirect calorimetry in dox-fed Tg-$^{AT\text{-}hA2}$;m$A2^{-/-}$, chow-fed WT, and Tg-$^{AT\text{-}hA2}$;m$A2^{-/-}$ mice

To comprehensively assess the energy regulation in Tg-$^{AT\text{-}hA2}$;m$A2^{-/-}$ mice, we measured the food and water intake, O_2 and CO_2 levels, and computed basal energy expenditure (EE), energy balance, and respiratory exchange ratio (RER) in these mice using indirect calorimetry methods. As previously reported in *Agpat2*$^{-/-}$ mice,[9] chow-fed Tg-$^{AT\text{-}hA2}$;m$A2^{-/-}$ male and female mice consumed more food (presented in kilocalories) than WT mice on similar chow diet and drank more water than WT mice, although this was more marked in females than in

Table 2. Protein measurements in the livers of 12-week chow-fed wild-type (WT) and chow-fed and doxycycline (dox)-fed Tg-$^{AT\text{-}hA2}$;m$A2^{-/-}$ male and female mice using tandem mass tag-mass spectrometry (TMT-MS)

Sex					Male					Female				
Genotype					WT	Tg-m$A2^{-/-}$				WT	Tg-m$A2^{-/-}$			
Protein name	Protein Accession	Peptide sequence [aa–aa]	PSM	Unique peptide #	Chow (n = 3)	Chow (n = 3)	Dox (n = 3)	Chow (n = 3)	Dox (n = 3)	Chow (n = 3)	Chow (n = 3)	Dox (n = 3)	Chow (n = 3)	Dox (n = 3)
Group comparison						A	B	C			A	B	C	
Insulin Signaling														
INSR	P15208	DIYETDYYR [1173–1181]	*14*	*7*	1	1.75[a]	1.57	1	0.90	1	2.85[b]	1.52[a]	1	0.54
IRS1	P35569	YIPGANLGTSPALPGDEAAGAADLDNR [489–515]	*10*	*6*	1	1.50	1.24	1	0.82	1	2.24[b]	1.18	1	0.53[a]
IRS2	P81122	VTLAPAGGALQHSR [413–426]	*3*	*3*	1	2.27[a]	1.84[a]	1	0.81	1	4.02[b]	1.76[a]	1	0.44
PIK3R4	Q8VD65	ETFLSADER [334–342]	*28*	*15*	1	1.28[a]	1.13	1	0.88	1	1.90[d]	1.14	1	0.60[b]
PDK1	Q8BFP9	ESFGVDPVTSQNVQYFLDR [165–183]	*28*	*11*	1	2.12[b]	1.10	1	0.52[b]	1	1.93[a]	1.35	1	0.70
PDK2	Q9JK42	ALSTDSVER [362–370]	*16*	*6*	1	1.87	1.26	1	0.67	1	2.26[b]	1.59	1	0.70
MTOR	Q9JLN9	DLELAVPGTYDPNQPIIR [2135–2152]	*89*	*35*	1	1.27	1.11	1	0.87	1	1.95[c]	1.10	1	0.56[c]
MEAK7	Q8K0P3	SVLDSNPEAR [423–432]	*4*	*3*	1	1.92[c]	1.27	1	0.66[c]	1	2.00[b]	1.05	1	0.52[b]
RICTOR	Q6QI06	HVPPPDDR [1448–1455]	*12*	*6*	1	1.22	1.23	1	1.01	1	2.33[c]	1.30[a]	1	0.56[b]
RPTOR	Q8K4Q0	IPEEHDLESQIR [974–985]	*20*	*10*	1	1.33[a]	1.12	1	0.84	1	1.84[c]	1.20[a]	1	0.65[b]
DEPTOR	Q570Y9	DDGTFALDSEVK [120–131]	*42*	*13*	1	1.89[d]	1.23[b]	1	0.65[b]	1	2.15[c]	1.20	1	0.56[b]
AKT2	Q60823	DIKLENLMLDKDGHIK [274–289]	*43*	*13*	1	1.86[d]	1.16	1	0.62[b]	1	2.20[d]	1.22[a]	1	0.55[c]
FOXO3	Q9WVH4	VQNEGTGK [222–229]	*4*	*3*	1	1.61[a]	1.37	1	0.85	1	2.24[c]	1.08	1	0.48[c]
GSK3A	Q2NL51	VTTVVATVGQGPER [100–113]	*8*	*4*	1	0.95	1.06	1	1.12	1	1.28[a]	1.03	1	0.80[a]
GSK3B	Q9WV60	DTPALFNFTTQELSSNPPLATILIPPHAR [335–383]	*10*	*6*	1	0.88	1.10	1	1.25	1	1.20	0.96	1	0.80
IGF Pathway														
IGFBP1	P47876	LAAAQQK [200–206]	*2*	*1*	1	0.27	0.70	1	2.58	1	1.10	1.78[a]	1	1.62
IGF1	P05017	GFYFNKPTGYGSSIR [70–84]	*3*	*2*	1	2.40	0.98	1	0.41	1	5.29[b]	1.07	1	0.20[b]

(*Continued on next page*)

Table 2. *Continued*

Sex					Male					Female				
Genotype					WT	Tg-m*A2*$^{-/-}$				WT	Tg-m*A2*$^{-/-}$			
Protein name	Protein Accession	Peptide sequence [aa–aa]	PSM	Unique peptide #	Chow (*n* = 3)	Chow (*n* = 3)	Dox (*n* = 3)	Chow (*n* = 3)	Dox (*n* = 3)	Chow (*n* = 3)	Chow (*n* = 3)	Dox (*n* = 3)	Chow (*n* = 3)	Dox (n = 3)
Group comparison						A	B	C			A	B	C	
Glucose Metabolism														
CHREBP	Q99MZ3	DQEGPVGLADFGPR [67–80]	*12*	*5*	1	3.27[b]	1.27	1	0.39[b]	1	3.86[b]	1.16	1	0.30[b]
PCK1	Q9Z2V4	NTIFTNVAETSDGGVYWEG IDEPLAPGVTITSWK [354–387]	*235*	*38*	1	1.58	1.39	1	0.88	1	2.52[a]	1.39	1	0.55
G6PC1	P35576	ILGQTHK [348–354]	*14*	*6*	1	1.13	1.06	1	0.94	1	0.74	1.03	1	1.39
PKLR	P52480; P53657	GDLGIEIPAEK [295–305], [338–348]	*448*	*40*	1	1.64[b]	1.00	1	0.61[b]	1	1.03	0.72	1	0.70
Insulin Modulation														
IDE	Q9JHR7	AIEDMTEEAFQK [873–884]	*132*	*41*	1	1.34[b]	1.04	1	0.77[a]	1	1.46[b]	1.08	1	0.74[b]

Shown are the fold changes in the proteins between the chow-fed WT and dox-fed Tg-AT-hA2;m*A2*$^{-/-}$ mice. The TMT-MS data are first normalized by total ion species for each sample, followed by a ratio of protein to GAPDH. Shown is a representative unique peptide that is detected for each protein consistently for both sexes. *p* values are determined by one-way ANOVA.

PSM, peptide-spectrum match; aa, amino acid. WT: Tg-AT-hA2;m*A2*$^{+/+}$. Tg-AT-hA2;m*A2*$^{-/-}$ is abbreviated to Tg-m*A2*$^{-/-}$.

[a]$p \leq 0.05$.

[b]$p \leq 0.01$.

[c]$p \leq 0.001$.

[d]$p \leq 0.0001$.

Table 3. Phosphoprotein measurements in the livers of 12-week chow-fed wild-type (WT) and chow-fed and doxycycline (dox)-fed Tg-$^{AT\text{-}hA2}$;m$A2^{-/-}$ male and female mice using tandem mass tag-mass spectrometry (TMT-MS)

Sex			Males						Females					
Genotype			WT		Tg-m$A2^{-/-}$		Tg-m$A2^{-/-}$		WT		Tg-m$A2^{-/-}$		Tg-m$A2^{-/-}$	
Diet (sample number)			Chow (n = 3)		Chow (n = 3)		Dox (n = 3)		Chow (n = 3)		Chow (n = 3)		Dox (n = 3)	
Protein symbol	Protein accession	Phosphopeptide detected [aa–aa]	Avg	SD	Avg	SD	Avg	SD	Avg	SD	Avg	SD	Avg	SD
RPTOR	Q8K4Q0	ILDTSSLTQSAPASPTNK [850–867]	6.30	0.73	7.87	2.26	8.52	0.36	6.21	0.44	7.66	1.67	6.54	1.13
AKT2	Q60823	CGSPSDSSTSEMMEVAVNK [124–142]	1.03	0.25	1.07	0.44	0.84	0.26	1.11	0.16	1.35	0.27	1.02	0.17
GSK3A	Q2NL51	GEPNVSYICSR [273–283]	0.87	0.62	0.89	0.71	0.82	0.38	1.35	0.46	1.52	0.01	1.48	0.05
CHREBP	Q99MZ3	VVPSPDSDSDTDLEDPSPR [17–35]	17.69	2.62	30.08[a]	6.30	16.90[b]	1.86	19.46	1.16	23.18[c]	2.31	18.42[d]	4.14
PCK1	Q9Z2V4	VIQGSLDSLPQAVR [15–28]	0.08	0.01	0.06	0.02	0.08	0.01	0.06	0.01	0.06	0.01	0.07	0.00

Shown is the normalized abundance of total protein that is phosphorylated in the proteins for each group studied. The TMT-MS data are first normalized by total ion species for each sample, followed by a ratio of protein to GAPDH. Shown is a representative unique phosphopeptide that is detected for each protein consistently for both sexes. p values are determined by one-way ANOVA.

PSM, peptide-spectrum match; aa, amino acid. WT: Tg-AT-hA2;m$A2^{+/+}$. Tg-AT-hA2;m$A2^{-/-}$ is abbreviated to Tg-m$A2^{-/-}$.

[a]Chow-fed WT vs. chow-fed Tg-AT-hA2;m$A2^{-/-}$ male mice p = 0.02.

[b]Chow-fed Tg-AT-hA2;m$A2^{-/-}$ vs. dox-fed Tg-AT-hA2;m$A2^{-/-}$ male mice p = 0.02.

[c]Chow-fed Tg-AT-hA2;m$A2^{-/-}$ vs. dox-fed Tg-AT-hA2;m$A2^{-/-}$ female mice. p = 0.01.

[d]Chow-fed WT vs. dox-fed Tg-AT-hA2;m$A2^{-/-}$ female mice p = 0.04.

males (Figures 4A–4D), possibly explaining why female livers were heavier. Interestingly, upon regeneration of AT in the Tg-$^{AT\text{-}hA2}$;m$A2^{-/-}$ background, dox-fed male Tg-$^{AT\text{-}hA2}$;m$A2^{-/-}$ mice consumed more calories compared to chow-fed Tg-$^{AT\text{-}hA2}$;m$A2^{-/-}$ mice, contrary to our expectation. Although female dox-fed Tg-$^{AT\text{-}hA2}$;m$A2^{-/-}$ mice consumed fewer calories than chow-fed Tg-$^{AT\text{-}hA2}$;m$A2^{-/-}$ mice, this did not reach statistical significance (Figures 4A and 4B). The water consumption in dox-fed Tg-$^{AT\text{-}hA2}$;m$A2^{-/-}$ mice returned to the levels of chow-fed WT mice (Figures 4C and 4D). This showed that although regeneration of AT in Tg-$^{AT\text{-}hA2}$;m$A2^{-/-}$ mice normalizes the water consumption to the levels of chow-fed WT mice, it does not normalize food intake levels.

As shown in the hourly plots for O_2 and CO_2, none of the genotypes studied showed any statistically significant changes in oxygen consumption or carbon dioxide production (Figures S9A–S9D). Additionally, we noted that the RER, a measure of fuel switching between fat and carbohydrate, did not vary between chow and dox-fed Tg-$^{AT\text{-}hA2}$;m$A2^{-/-}$ mice but differed from that in chow-fed WT mice. This primarily occurred during the dark cycle for both sexes, predominantly coinciding with the period when the mice were eating (Figures 4E and 4F). An RER near 0.7 indicates that fat is the predominant fuel source, while a value of 1.0 is indicative of carbohydrates predominance. A value between 0.7 and 1.0 suggests a mix of both fats and carbohydrates. While chow-fed WT mice switched their fuel source between fats and carbohydrates, as expected, chow- and dox-fed Tg-$^{AT\text{-}hA2}$;m$A2^{-/-}$ mice maintained an RER around 0.8 throughout the duration of the experiment, reflecting a constant use of a mix of both fats and carbohydrates.

The concept of energy balance pertains to the balance of energy intake versus EE. If the energy intake and expenditure are equal, the energy balance becomes close to zero. However, when the EE is more than the energy intake, the energy balance becomes negative. This energy balance is dependent on several factors, including the animal ambulatory and locomotor activities, body mass, food intake, and in our murine model, the presence or absence of AT. Surprisingly, the ambulatory activity of these mice showed no statistically significant difference among any of the three groups of mice (Figures S9I–S9L). When compared to chow-fed Tg-$^{AT\text{-}hA2}$;m$A2^{-/-}$ mice, the EE of dox-fed Tg-$^{AT\text{-}hA2}$;m$A2^{-/-}$ mice increased in both sexes, albeit to a lesser extent than that in female mice (Figures 4G, 4H, S9E, and S9F). Energy balance was calculated as food intake minus EE. Based on this, chow-fed Tg-$^{AT\text{-}hA2}$;m$A2^{-/-}$ mice had a larger positive cumulative energy balance than either chow-fed WT or dox-fed Tg-$^{AT\text{-}hA2}$;m$A2^{-/-}$ mice in both sexes (Figures 4I, 4J, S9G, and S9H), which reflected that chow-fed Tg-$^{AT\text{-}hA2}$;m$A2^{-/-}$ mice consumed more calories to chow-fed WT mice but their EE remained comparable. This may explain how the body weight of chow-fed Tg-$^{AT\text{-}hA2}$;m$A2^{-/-}$ mice could catch up to that of the chow-fed WT and dox-fed Tg-$^{AT\text{-}hA2}$;m$A2^{-/-}$ mice (Figure S3). However, it was difficult to ascertain which organs had the excess energy stored or whether there was excessive thermogenesis in other organs like skeletal muscles (i.e., shivering) using the indirect calorimetry method. However, chow-fed Tg-$^{AT\text{-}hA2}$;m$A2^{-/-}$ mice lacked brown AT, known for thermogenesis. While it was possible that the excess energy balance was being stored as fat in the liver, it did not translate to an increase in body mass (Figures 4I–4L).

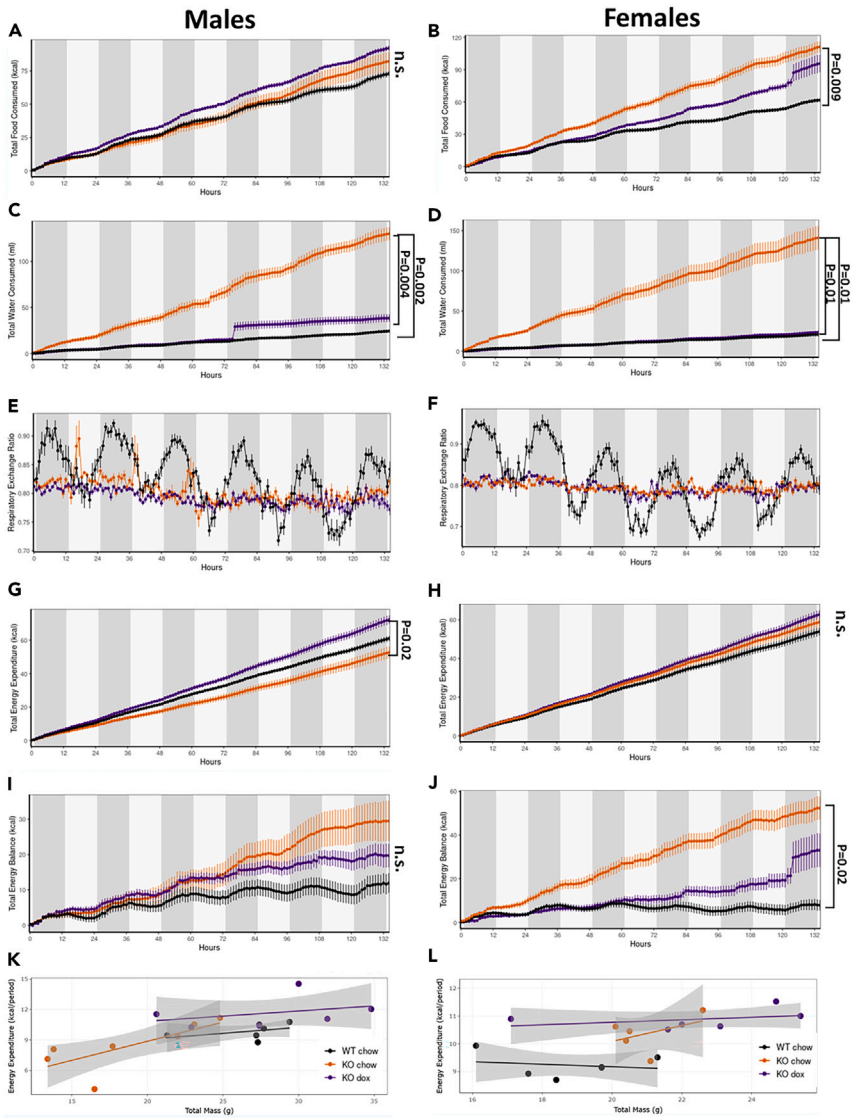

Figure 4. Food and water intake and indirect calorimetric measurements at 12 weeks in chow- and dox-fed Tg-$^{AT\text{-}hA2}$;m$A2^{-/-}$ mice

Shown are the screenshots of the graphs of indirect calorimetric measurements.

(A and B) Cumulative food intake for 12-week (A) males and (B) females.

(C and D) Cumulative water intake for 12-week (C) males and (D) females.

(E and F) Hourly respiratory exchange ratio (RER) for 12-week (E) males and (F) females over four days. Note that while wild type (WT) mice switch between the fuel source (carbohydrates at night and fat during the day), both the chow- and dox-fed Tg-$^{AT\text{-}hA2}$;m$A2^{-/-}$ mice are constantly utilizing a mixture of carbohydrates and fat.

(G and H) The resting total energy expenditure (TEE) for (G) males and (H) females show increased TEE in dox-fed Tg-$^{AT\text{-}hA2}$;m$A2^{-/-}$ mice compared to that in chow fed Tg-$^{AT\text{-}hA2}$;m$A2^{-/-}$ mice, but this relationship is found only in male mice.

(I and J) Total energy balance (TEB) for (I) males and (J) females. Dox-fed Tg-$^{AT\text{-}hA2}$;m$A2^{-/-}$ mice show positive TEB to those of WT, but less than chow-fed Tg-$^{AT\text{-}hA2}$;m$A2^{-/-}$ mice.

(K and L) (K) Male and (L) female dox-fed Tg-$^{AT\text{-}hA2}$;m$A2^{-/-}$ mice have improved energy expenditure profiles compared to that in chow-fed Tg-$^{AT\text{-}hA2}$;m$A2^{-/-}$ mice. Dark hours are shaded in gray, light hours are in white. All measurements are tabulated for total body weight, see text for explanation. $n = 6$ per group. These measurements are performed in two separate experiments ($n = 3$) and the data are combined for tabulation, and analyzed using CalR, a web-based analysis tool for indirect calorimetry experiments. Data are represented as mean ± SEM. p values for (A–J) are determined using one-way ANOVA. For additional statistics calculated in the CalR program, see Table S2 n.s., not significant. WT: Tg-$^{AT\text{-}hA2}$;m$A2^{+/+}$. Tg-$^{AT\text{-}hA2}$;m$A2^{-/-}$ abbreviated to Tg-m$A2^{-/-}$. See also Figure S9.

The regression analysis displayed in Figures 4K and 4L shows the relationship between EE and body mass; as the body mass increased, the EE increased. We demonstrated this relationship using total body mass normalization because in chow-fed Tg-$^{AT\text{-}hA2}$;m$A2^{-/-}$ mice, there was no AT (lipodystrophy). Although AT did not contribute directly toward the EE, the adipokines (e.g., leptin) secreted from the AT exerted a positive (indirect) effect. Under these circumstances, the relationship of AT and muscle mass became skewed as they were involved in energy storage and expenditure, respectively. Regardless of which normalization method was used, the relationship between the groups remained the same. The relationship between EE and body mass was different between males and females in our study. For the males, all three groups showed a positive relationship; as the body mass increased, the EE also increased. However, chow-fed female WT mice had a slightly negative energy slope (i.e., as the body mass increased, the EE did not increase), whereas chow-fed and dox-fed Tg-$^{AT\text{-}hA2}$;m$A2^{-/-}$ mice both exhibited positive energy slopes.

DISCUSSION

In this study, although the regenerated AT in dox-fed *Tg-$^{AT\text{-}hA2}$;m$A2^{-/-}$* mice was only ~30–50% of that in WT mice,[16] dox-fed *Tg-$^{AT\text{-}hA2}$;m$A2^{-/-}$* mice demonstrated amelioration of hepatic steatosis. We chose to study 12- and 24-week-old dox-fed Tg-$^{AT\text{-}hA2}$;m$A2^{-/-}$ mice of both sexes, where the presence of AT was detectable. Upon AT regeneration by 12 weeks in dox-fed Tg-$^{AT\text{-}hA2}$;m$A2^{-/-}$ mice, we began to notice a decrease in liver weight and TAG and AST levels in both sexes, accompanied by reduced expression of transcripts for the key enzymes in the *de novo* lipogenesis of TAG synthesis, mitochondrial metabolism, and gluconeogenesis, albeit with females responding better than males. Despite only a partial regeneration of adipose depots, the reduction in hepatic TAG levels was substantial, suggesting that even a small amount of AT is consequential for regulating hepatic TAG levels for both sexes.

There are multiple pathways for the development of hepatic steatosis, with IR being a prominent factor among them. A systemic IR involves the central nervous system and several peripheral organs (liver, skeletal muscles, AT, and pancreas). Additionally, a new study indicates that the gut could communicate with the brain via spinal sensory neurons, bypassing the vagal nerves.[24] Understanding IR has been the goal of several investigations; however, it has not been fully understood. A recent study in mice showed that the most critical peripheral tissues were skeletal muscles (soleus and extensor digitorum longus) and white AT (WAT; epigonadal).[25] The most insulin-sensitive tissue for glucose uptake in mice, regardless of genetic background, is the epigonadal WAT.[25] While the development of IR can occur in animals who have these tissues intact (such as IR seen in obese individuals with excess AT), it can also develop when there is total loss of AT in conditions such as congenital generalized lipodystrophy in humans and mice. Loss of AT also results in loss of adipokines, specifically leptin, which regulates satiety and, consequently, food (calorie) intake. A general paradigm for IR is that an increase in plasma insulin suppresses liver gluconeogenesis, increases synthesis of TAG in AT, and increases glucose disposal through skeletal muscles. An unanticipated result of this paradigm is that livers of IR animals continue to synthesize lipids,[26] a mechanism that is still not fully understood. A dissociation of IR and hepatic steatosis was also shown in the livers of mice overexpressing *Dgat2*.[27] Measurement of IR in whole animals mostly revolves around plasma glucose and insulin, and various methods exist to calculate the ratios as part of IR assessment. In normal animals, food intake (calorie intake) is primarily regulated by leptin, a regulatory factor that is lost in lipodystrophic animals. Therefore, uncontrolled food intake increases the systemic load of glucose levels, resulting in dysfunctional pancreas (increased insulin secretion), skeletal muscles, and liver. When we examined the non-fasting plasma glucose and insulin levels in 12- and 24-week chow- and dox-fed *Tg-$^{AT\text{-}hA2}$;m$A2^{-/-}$* mice in a setting of unrestricted food intake, food intake increased in chow-fed *Tg-$^{AT\text{-}hA2}$;m$A2^{-/-}$* mice (Figures 4A and 4B), and the plasma insulin levels markedly increased (Table 4). However, with 6 h of fasting, chow- and dox-fed *Tg-$^{AT\text{-}hA2}$;m$A2^{-/-}$* mice had plasma glucose levels more akin to those observed in WT mice, but the plasma insulin levels remained comparatively high in both sexes in the chow-fed *Tg-$^{AT\text{-}hA2}$;m$A2^{-/-}$* mice. The plasma insulin levels of dox-fed *Tg-$^{AT\text{-}hA2}$;m$A2^{-/-}$* mice were lower compared to those in chow-fed *Tg-$^{AT\text{-}hA2}$;m$A2^{-/-}$* mice; however, they were not as low as those seen in the WT mice. If the fasting glucose levels were low, why are the plasma insulin levels of chow-fed *Tg-$^{AT\text{-}hA2}$;m$A2^{-/-}$* mice not returning to WT levels? Is the relationship between fasting blood glucose and insulin lost or is there an inherent defect in the pancreas of chow-fed Tg-$^{AT\text{-}hA2}$;m$A2^{-/-}$ mice for secreting insulin? The secretion of insulin involves multiple steps where (1) the insulin granules are packed in a vesicle coated mostly by phospholipids, (2) the vesicles are fused with the plasma membrane, and (3) the cargo (insulin) is released. AGPAT2, an enzyme that synthesizes PA, a phospholipid that is the substrate for other phospholipids, could potentially play a role in this process. In this regard, it is important to note that the pancreas also expresses a high level of AGPAT2, second only to AT, in WT mice (Figure S10). Pancreas-specific re-expression of AGPAT2 in *Agpat2$^{-/-}$* mice might resolve this argument.

Excessive energy intake because of leptin deficiency seems to be the main cause of IR in lipodystrophic mice. In fact, administration of recombinant leptin (metreleptin) to lipodystrophic humans[28] and mice[29] results in amelioration of several features of IR. However, this does not seem to involve the liver. We genetically deleted the hepatic leptin receptor in *Agpat2$^{-/-}$* mice;[30] however, when leptin was administered, hepatic steatosis and IR still decreased. Lipodystrophic mice exhibit a state of increased blood glucose and insulin levels due to constant energy consumption (food intake) and reach a state of systemic IR. From the current murine studies, we note that chow-fed *Tg-$^{AT\text{-}hA2}$;m$A2^{-/-}$* mice are still hyperinsulinemic even when they are fasted, despite the plasma glucose levels being no different than WT mice. This study suggests that in lipodystrophic humans, restrictive calorie intake should decrease the plasma glucose and insulin levels, IR, and hepatic steatosis.

Notably, the current study revealed differences between sexes in the biological response to the tests conducted. Initially, we analyzed the datasets by sex interaction for each experimental outcome to measure how similar the males and females were for that specific "trait." Here, we defined "traits" as differences in male-female body weight, plasma glucose, TAG levels, and insulin levels, among others. At

Table 4. Relationship of fasting and non-fasting plasma glucose and insulin levels in wild-type (WT) and chow- and dox-fed Tg-$^{AT\text{-}hA2}$;m$A2^{-/-}$ male and female mice

Age	12 weeks					
Genotype	WT		Tg-m$A2^{-/-}$ chow		Tg-m$A2^{-/-}$ dox	
	Non-fasting	Fasting (T_0)	Non-fasting	Fasting (T_0)	Non-fasting	Fasting (T_0)
Sex	Male					
Glucose (mg/dL)	306.43 ± 29.82	172.50 ± 45.66	378.50 ± 247.48	127.17 ± 76.39	297.57 ± 54.23	168.67 ± 56.50
Insulin (ng/mL)	0.43 ± 0.06	0.89 ± 0.52	14.55 ± 22.25	2.94 ± 2.33	2.62 ± 1.72	1.61 ± 1.17
Glucose/Insulin	720.83 ± 75.25	239.44 ± 105.79	93.87 ± 86.20	61.83 ± 42.38	161.79 ± 99.47	160.30 ± 95.20
Sex	Female					
Glucose (mg/dL)	259.80 ± 19.15	141.00 ± 23.32	532.15 ± 97.38	162.33 ± 91.57	289.57 ± 36.92	141.83 ± 41.65
Insulin (ng/mL)	0.68 ± 0.34	0.36 ± 0.10	25.18 ± 25.97	4.08 ± 2.31	2.55 ± 1.07	0.75 ± 0.47
Glucose/Insulin	468.36 ± 230.65	415.99 ± 126.06	134.48 ± 205.71	50.27 ± 29.71	133.35 ± 67.98	219.13 ± 77.90
Age	24 weeks					
Genotype	WT		Tg-m$A2^{-/-}$ chow		Tg-m$A2^{-/-}$ dox	
	Non-fasting	Fasting (T_0)	Non-fasting	Fasting (T_0)	Non-fasting	Fasting (T_0)
Sex	Male					
Glucose (mg/dL)	262.33 ± 23.71	159.00 ± 35.59	345.20 ± 98.67	154.67 ± 8.96	260.75 ± 25.43	122.80 ± 22.33
Insulin (ng/mL)	0.45 ± 0.12	0.70 ± 0.24	35.22 ± 21.74	14.40 ± 10.47	7.53 ± 3.71	7.83 ± 6.36
Glucose/Insulin	600.26 ± 123.35	236.20 ± 33.97	12.88 ± 6.59	20.56 ± 21.51	40.04 ± 15.14	26.15 ± 17.29
Sex	Female					
Glucose (mg/dL)	233.40 ± 5.81	150.33 ± 16.50	534.60 ± 39.83	233.80 ± 172.75	292.60 ± 93.22	178.33 ± 72.45
Insulin (ng/mL)	0.53 ± 0.22	0.57 ± 0.20	30.29 ± 25.26	4.67 ± 1.40	3.47 ± 2.99	1.04 ± 0.67
Glucose/Insulin	558.09 ± 165.85	295.70 ± 150.55	31.41 ± 25.99	51.82 ± 40.41	175.46 ± 138.27	217.49 ± 109.97

Shown are the plasma glucose and plasma insulin levels in fasting and non-fasting mice of both sexes at 12 and 24 weeks and the ratio of glucose/insulin calculations as a measure of insulin resistance (IR). These data were extracted from Figures 2, 3, S5, and S6 to emphasize the relationship between plasma insulin and glucose levels, hyperinsulinemia, and IR. Data are represented as mean ± SD.

times, we observed sex-interactions, while on other occasions, we did not. Generally, we observed inconsistent differences in the metabolic pathways between males and females; therefore, this study did not provide a unified factor that is responsible for the sex differences noted. Furthermore, adult animals, including humans, have different sex hormones and different genetics (XY and XX genotype in males and females, respectively) which can alter physiological traits such as those related to metabolism. For example, testosterone, a well-known anabolic hormone present mostly in males, exerts distinct metabolic effects in males compared to that in females. We could not exclude testosterone from the mice without additional manipulations in making this observation. To measure the influence of sex hormones, we would need to perform experiments in mice that have undergone orchiectomy and ovariectomy for males and females, respectively.[31] However, in each of these experimental settings, the data that emerge will be difficult to extrapolate to the human condition. A recent study examined the gene expression in five tissues, including the liver, throughout development and neonatal stages in both sexes of humans and other vertebrates. The findings led to the conclusion that there is a sex-specific gene expression pattern in each of the studied species.[32] This study suggests that there are specific gene expression patterns between males and females that result in differences in metabolism and other biological processes.

Overall, we showed that only a small amount of AT regeneration was required to ameliorate hepatic steatosis in both sexes which is beneficial for lipodystrophic mice and potentially humans. However, based on the sex-dependent responses noted in this study, the applicability of these findings may be more relevant to human females with CGL, type 1. Nevertheless, it is essential to conduct more detailed investigations to assess sex-dependent outcomes in humans. Additionally, the re-expression of AGPAT2 embryonically in humans currently poses technical challenges that need to be addressed.

Limitations of the study

A limitation of this study was that h*AGPAT2* re-expression was restricted to the AT in *Agpat2*$^{-/-}$ mice. In contrast, endogenous *AGPAT2* is expressed in various tissues, including the liver, pancreas, and mouse mammary glands (at low levels). The generation of either a liver-specific or global transgenic h*AGPAT2* murine model will confirm the role of *AGPAT2* expression in tissues other than the AT and elucidate the

cross-tissue interaction between the liver and pancreas. Although this study was not specifically designed for such an investigation, it did not account for the contribution of endogenous *AGPAT2* in cross-tissue effects, such as the liver-AT or liver-AT-pancreas axes. An additional limitation arose when studying insulin sensitivity and response in chow-fed Tg-$^{AT\text{-}hA2}$;m*A2*$^{-/-}$ mice. Gathering data to compare with the dox-fed mice was very difficult because the chow-fed Tg-$^{AT\text{-}hA2}$;m*A2*$^{-/-}$ mice already possessed high insulin levels and were highly insulin-resistant. Therefore, we were unable to quantitatively determine the extent to which the insulin sensitivity of dox-fed Tg-$^{AT\text{-}hA2}$;m*A2*$^{-/-}$ mice may have improved. Furthermore, this study was not designed to elucidate the sex differences between males and females in metabolic outcomes. As discussed, additional studies are required to define the molecular mechanisms underlying the differences between both sexes.

STAR★METHODS

Detailed methods are provided in the online version of this paper and include the following:

- KEY RESOURCES TABLE
- RESOURCE AVAILABILITY
  - Lead contact
  - Materials availability
  - Data and code availability
- EXPERIMENTAL MODEL AND STUDY PARTICIPANT DETAILS
- METHOD DETAILS
  - Brief description of generation of Tg-$^{AT\text{-}hA2}$;m*A2*$^{-/-}$ mice
  - Mouse genotyping
  - Mouse genetic background testing
  - Oral glucose tolerance test (OGTT)
  - Insulin tolerance test (ITT)
  - Homeostatic model assessment of insulin resistance (HOMA-IR)
  - Indirect calorimetry
  - Plasma metabolite measurements
  - Plasma insulin assay
  - Triacylglycerol (TAG) assay
  - Total RNA isolation
  - Reverse transcription quantitative polymerase chain reaction (RT-qPCR)
  - Quantitative PCR using pooled sample strategy
  - Tandem mass Tag-Mass Spectrometry (TMT-MS) for liver
- QUANTIFICATION AND STATISTICAL ANALYSIS

SUPPLEMENTAL INFORMATION

Supplemental information can be found online at https://doi.org/10.1016/j.isci.2024.109517.

ACKNOWLEDGMENTS

National Institutes of Health Grants, R01- DK105448, Nutrition and Obesity Research Center, National Institutes of Health, P30 DK127984, and the Southwestern Medical Foundation supported this work. The content is solely the responsibility of the authors and does not necessarily represent the official views of the National Institutes of Health. The authors thank members of the mouse metabolic core at University of Texas Southwestern Medical Center for indirect calorimetric assays; William Bernard and Alexander Banks at Harvard Medical School, Boston, MA, for their assistance with the CalR program; the UTSW Proteomics Core for assistance with proteomics experiments; Xilong Li for providing additional statistical analysis; and Taconic Biosciences for determining the mouse genetic background. We would like to thank Editage for English language editing (www.editage.com).

AUTHOR CONTRIBUTIONS

A.K.A. designed, supervised, helped collect data, analyzed the data, and wrote the first draft. K.T. collected most of the data, prepared figures and copyedited the manuscript. J.D.H. and A.G. reviewed the manuscript and provided comments. All authors reviewed and edited the manuscript.

DECLARATION OF INTERESTS

The authors declare no competing interests.

Received: February 21, 2023
Revised: January 22, 2024
Accepted: March 14, 2024
Published: March 26, 2024

REFERENCES

1. Agarwal, A.K., and Garg, A. (2006). Genetic basis of lipodystrophies and management of metabolic complications. Annu. Rev. Med. *57*, 297–311. https://doi.org/10.1146/annurev.med.57.022605.114424.
2. Agarwal, A.K., and Garg, A. (2006). Genetic disorders of adipose tissue development, differentiation, and death. Annu. Rev. Genom. Hum. Genet. *7*, 175–199. https://doi.org/10.1146/annurev.genom.7.080505.115715.
3. Garg, A., and Agarwal, A.K. (2009). Lipodystrophies: disorders of adipose tissue biology. Biochim. Biophys. Acta *1791*, 507–513. https://doi.org/10.1016/j.bbalip.2008.12.014.
4. Hammarstedt, A., Graham, T.E., and Kahn, B.B. (2012). Adipose tissue dysregulation and reduced insulin sensitivity in non-obese individuals with enlarged abdominal adipose cells. Diabetol. Metab. Syndr. *4*, 42. https://doi.org/10.1186/1758-5996-4-42.
5. Eslam, M., Newsome, P.N., Sarin, S.K., Anstee, Q.M., Targher, G., Romero-Gomez, M., Zelber-Sagi, S., Wai-Sun Wong, V., Dufour, J.F., Schattenberg, J.M., et al. (2020). A new definition for metabolic dysfunction-associated fatty liver disease: An international expert consensus statement. J. Hepatol. *73*, 202–209. https://doi.org/10.1016/j.jhep.2020.03.039.
6. Rinella, M.E., Neuschwander-Tetri, B.A., Siddiqui, M.S., Abdelmalek, M.F., Caldwell, S., Barb, D., Kleiner, D.E., and Loomba, R. (2023). AASLD Practice Guidance on the clinical assessment and management of nonalcoholic fatty liver disease. Hepatology *77*, 1797–1835. https://doi.org/10.1097/HEP.0000000000000323.
7. Kokkorakis, M., Boutari, C., Katsiki, N., and Mantzoros, C.S. (2023). From non-alcoholic fatty liver disease (NAFLD) to steatotic liver disease (SLD): an ongoing journey towards refining the terminology for this prevalent metabolic condition and unmet clinical need. Metabolism *147*, 155664. https://doi.org/10.1016/j.metabol.2023.155664.
8. Song, S.J., Lai, J.C.T., Wong, G.L.H., Wong, V.W.S., and Yip, T.C.F. (2024). Can we use old NAFLD data under the new MASLD definition? J. Hepatol. *80*, e54–e56. https://doi.org/10.1016/j.jhep.2023.07.021.
9. Cortés, V.A., Curtis, D.E., Sukumaran, S., Shao, X., Parameswara, V., Rashid, S., Smith, A.R., Ren, J., Esser, V., Hammer, R.E., et al. (2009). Molecular mechanisms of hepatic steatosis and insulin resistance in the AGPAT2-deficient mouse model of congenital generalized lipodystrophy. Cell Metab. *9*, 165–176. https://doi.org/10.1016/j.cmet.2009.01.002.
10. Agarwal, A.K. (2012). Lysophospholipid acyltransferases: 1-acylglycerol-3-phosphate O-acyltransferases. From discovery to disease. Curr. Opin. Lipidol. *23*, 290–302. https://doi.org/10.1097/MOL.0b013e328354fcf4.
11. Zhang, Y., Proenca, R., Maffei, M., Barone, M., Leopold, L., and Friedman, J.M. (1994). Positional cloning of the mouse obese gene and its human homologue. Nature *372*, 425–432. https://doi.org/10.1038/372425a0.
12. Turner, N., Kowalski, G.M., Leslie, S.J., Risis, S., Yang, C., Lee-Young, R.S., Babb, J.R., Meikle, P.J., Lancaster, G.I., Henstridge, D.C., et al. (2013). Distinct patterns of tissue-specific lipid accumulation during the induction of insulin resistance in mice by high-fat feeding. Diabetologia *56*, 1638–1648. https://doi.org/10.1007/s00125-013-2913-1.
13. Agarwal, A.K., and Garg, A. (2003). Congenital generalized lipodystrophy: significance of triglyceride biosynthetic pathways. Trends Endocrinol. Metab. *14*, 214–221.
14. Coleman, R.A., and Lee, D.P. (2004). Enzymes of triacylglycerol synthesis and their regulation. Prog. Lipid Res. *43*, 134–176.
15. Yen, C.L.E., Stone, S.J., Cases, S., Zhou, P., and Farese, R.V., Jr. (2002). Identification of a gene encoding MGAT1, a monoacylglycerol acyltransferase. Proc. Natl. Acad. Sci. USA *99*, 8512–8517. https://doi.org/10.1073/pnas.132274899.
16. Agarwal, A.K., Tunison, K., Vale, G., McDonald, J.G., Li, X., Scherer, P.E., Horton, J.D., and Garg, A. (2023). Regulated adipose tissue-specific expression of human AGPAT2 in lipodystrophic Agpat2-null mice results in regeneration of adipose tissue. iScience *26*, 107806. https://doi.org/10.1016/j.isci.2023.107806.
17. Agarwal, A.K., Tunison, K., Vale, G., McDonald, J.G., Li, X., Horton, J.D., and Garg, A. (2024). Adipose-specific overexpression of human AGPAT2 in mice causes increased adiposity and mild hepatic dysfunction. iScience *27*, 108653. https://doi.org/10.1016/j.isci.2023.108653.
18. Sun, K., Wernstedt Asterholm, I., Kusminski, C.M., Bueno, A.C., Wang, Z.V., Pollard, J.W., Brekken, R.A., and Scherer, P.E. (2012). Dichotomous effects of VEGF-A on adipose tissue dysfunction. Proc. Natl. Acad. Sci. USA *109*, 5874–5879. https://doi.org/10.1073/pnas.1200447109.
19. Park, S.Y., Gautier, J.F., and Chon, S. (2021). Assessment of Insulin Secretion and Insulin Resistance in Human. Diabetes Metab. J. *45*, 641–654. https://doi.org/10.4093/dmj.2021.0220.
20. Haeusler, R.A., McGraw, T.E., and Accili, D. (2018). Biochemical and cellular properties of insulin receptor signalling. Nat. Rev. Mol. Cell Biol. *19*, 31–44. https://doi.org/10.1038/nrm.2017.89.
21. Régnier, M., Carbinatti, T., Parlati, L., Benhamed, F., and Postic, C. (2023). The role of ChREBP in carbohydrate sensing and NAFLD development. Nat. Rev. Endocrinol. *19*, 336–349. https://doi.org/10.1038/s41574-023-00809-4.
22. Belfiore, A., Malaguarnera, R., Vella, V., Lawrence, M.C., Sciacca, L., Frasca, F., Morrione, A., and Vigneri, R. (2017). Insulin Receptor Isoforms in Physiology and Disease: An Updated View. Endocr. Rev. *38*, 379–431. https://doi.org/10.1210/er.2017-00073.
23. Najjar, S.M., and Perdomo, G. (2019). Hepatic Insulin Clearance: Mechanism and Physiology. Physiology *34*, 198–215. https://doi.org/10.1152/physiol.00048.2018.
24. Zhang, T., Perkins, M.H., Chang, H., Han, W., and de Araujo, I.E. (2022). An inter-organ neural circuit for appetite suppression. Cell *185*, 2478–2494.e28. https://doi.org/10.1016/j.cell.2022.05.007.
25. Nelson, M.E., Madsen, S., Cooke, K.C., Fritzen, A.M., Thorius, I.H., Masson, S.W.C., Carroll, L., Weiss, F.C., Seldin, M.M., Potter, M., et al. (2022). Systems-level analysis of insulin action in mouse strains provides insight into tissue- and pathway-specific interactions that drive insulin resistance. Cell Metab. *34*, 227–239.e6. https://doi.org/10.1016/j.cmet.2021.12.013.
26. Brown, M.S., and Goldstein, J.L. (2008). Selective versus total insulin resistance: a pathogenic paradox. Cell Metab. *7*, 95–96. https://doi.org/10.1016/j.cmet.2007.12.009.
27. Monetti, M., Levin, M.C., Watt, M.J., Sajan, M.P., Marmor, S., Hubbard, B.K., Stevens, R.D., Bain, J.R., Newgard, C.B., Farese, R.V., Sr., et al. (2007). Dissociation of hepatic steatosis and insulin resistance in mice overexpressing DGAT in the liver. Cell Metab. *6*, 69–78. https://doi.org/10.1016/j.cmet.2007.05.005.
28. Oral, E.A., Simha, V., Ruiz, E., Andewelt, A., Premkumar, A., Snell, P., Wagner, A.J., DePaoli, A.M., Reitman, M.L., Taylor, S.I., et al. (2002). Leptin-replacement therapy for lipodystrophy. N. Engl. J. Med. *346*, 570–578. https://doi.org/10.1056/NEJMoa012437.
29. Shimomura, I., Hammer, R.E., Ikemoto, S., Brown, M.S., and Goldstein, J.L. (1999). Leptin reverses insulin resistance and diabetes mellitus in mice with congenital lipodystrophy. Nature *401*, 73–76. https://doi.org/10.1038/43448.
30. Cortés, V.A., Cautivo, K.M., Rong, S., Garg, A., Horton, J.D., and Agarwal, A.K. (2014). Leptin ameliorates insulin resistance and hepatic steatosis in Agpat2-/- lipodystrophic mice independent of hepatocyte leptin receptors. J. Lipid Res. *55*, 276–288. https://doi.org/10.1194/jlr.M045799.
31. Mauvais-Jarvis, F., Arnold, A.P., and Reue, K. (2017). A Guide for the Design of Pre-clinical Studies on Sex Differences in Metabolism. Cell Metab. *25*, 1216–1230. https://doi.org/10.1016/j.cmet.2017.04.033.
32. Rodríguez-Montes, L., Ovchinnikova, S., Yuan, X., Studer, T., Sarropoulos, I., Anders, S., Kaessmann, H., and Cardoso-Moreira, M. (2023). Sex-biased gene expression across mammalian organ development and evolution. Science *382*, eadf1046. https://doi.org/10.1126/science.adf1046.
33. Agarwal, A.K., Sukumaran, S., Cortés, V.A., Tunison, K., Mizrachi, D., Sankella, S., Gerard, R.D., Horton, J.D., and Garg, A. (2011). Human 1-acylglycerol-3-phosphate O-acyltransferase isoforms 1 and 2: biochemical characterization and inability to

rescue hepatic steatosis in Agpat2(-/-) gene lipodystrophic mice. J. Biol. Chem. *286*, 37676–37691. https://doi.org/10.1074/jbc.M111.250449.

34. Mina, A.I., LeClair, R.A., LeClair, K.B., Cohen, D.E., Lantier, L., and Banks, A.S. (2018). CalR: A Web-Based Analysis Tool for Indirect Calorimetry Experiments. Cell Metab. *28*, 656–666.e1. https://doi.org/10.1016/j.cmet.2018.06.019.

35. Agarwal, A.K., Tunison, K., Mitsche, M.A., McDonald, J.G., and Garg, A. (2019). Insights into lipid accumulation in skeletal muscle in dysferlin-deficient mice. J. Lipid Res. *60*, 2057–2073. https://doi.org/10.1194/jlr.RA119000399.

36. Sankella, S., Garg, A., and Agarwal, A.K. (2017). Activation of Sphingolipid Pathway in the Livers of Lipodystrophic Agpat2(-/-) Mice. J. Endocr. Soc. *1*, 980–993. https://doi.org/10.1210/js.2017-00157.

37. Navarrete-Perea, J., Yu, Q., Gygi, S.P., and Paulo, J.A. (2018). Streamlined Tandem Mass Tag (SL-TMT) Protocol: An Efficient Strategy for Quantitative (Phospho)proteome Profiling Using Tandem Mass Tag-Synchronous Precursor Selection-MS3. J. Proteome Res. *17*, 2226–2236. https://doi.org/10.1021/acs.jproteome.8b00217.

STAR★METHODS

KEY RESOURCES TABLE

REAGENT or RESOURCE	SOURCE	IDENTIFIER
Antibodies		
AGPAT2	Genway Biotech (custom made)	Agarwal et al., 2011[33]
Biological samples		
Liver tissue and plasma	This study	N/A
Chemicals, peptides, and recombinant proteins		
RNA Stat-60	Fisher Scientific	Cat# nc9489785
Protease + phosphatase inhibitors	Thermo Scientific	Cat# A32959
Sybr Green	Thermo Fisher	Cat# 4364346
Critical commercial assays		
RNeasy lipid mini extraction kit	Qiagen	Cat# 74804
DC Protein Assay Reagents Package	Bio-Rad	Cat# 5000116
Triglyceride Colorimetric Assay Kit	Cayman Chemical	Cat# 10010303
DNA-free™ DNA Removal Kit	Fisher Scientific	Cat# am1906
Reverse Transcription Reagents kit	Fisher Scientific	Cat# N8080234
Bovine insulin	Sigma-Aldrich	Cat# I0516-5ML
Mouse Insulin ELISA Kit	Crystal Chem	Cat# 90080
TMTpro™ 18-plex Label Reagent Set	Thermo Scientific	Cat# A52047
Pierce High pH Reversed-Phase Peptide Fractionation Kit	Thermo Scientific	Cat # 84868
High-select TiO2 phosphopeptide enrichment kit	Thermo Scientific	Cat# A32993
High-select Fe-NTA phosphopeptide enrichment kit	Thermo Scientific	Cat# A32992
Vitros 250 analyzer glucose slide	Ortho Clinical Diagnostics	Cat # 1707801
Vitros 250 analyzer triglyceride slide	Ortho Clinical Diagnostics	Cat # 1336544
Vitros 250 analyzer AST slide	Ortho Clinical Diagnostics	Cat # 8433815
Experimental models: Organisms/strains		
Mouse: Agpat2$^{-/-}$	In house	Cortés et al., 2009[9]
Mouse: rtTA-adiponectin	In house	Sun et al., 2012[18]
Mouse: Tg-AT-hA2; mA2$^{-/-}$	This paper	N/A
Oligonucleotides		
A full list of qPCR primers, see Table S3	This paper	N/A
Primer manufacturer	Integrated DNA Technologies	Coralville, IA
Primer manufacturer	Realtimeprimer.com	Elkin Park, PA
Recombinant DNA		
pBluescript-TRE-Tight	In house	Sun et al., 2012[18]
Software and algorithms		
GraphPad Prism version 9.2.0	GraphPad Software	https://www.graphpad.com
SAS version 9.4	SAS institute	https://www.sas.com
Proteome Discoverer v.3.0 SP1	Thermo Scientific	https://www.thermofisher.com
CalR Version 1.3	Harvard Digestive Diseases Center	https://calrapp.org/
Other		
Doxycycline diet	Bio-Serv	Cat# S4107
Normal chow diet	Envigo	Cat# 2916

(*Continued on next page*)

Continued

REAGENT or RESOURCE	SOURCE	IDENTIFIER
2.0 mL prefilled Bead Ruptor tube (2.8 mm ceramic beads)	Omni International	Cat# 19-628
TSE LabMaster	TSE Systems	https://www.tse-systems.com/metabolism/
Zirconium oxide beads 1.4 mm diameter	Thermo Fisher Scientific	Cat# 50-154-2945
StepOne Plus Real-Time PCR System	Thermo Fisher Scientific	Waltham, MA
Bullet Blender	Next Advance	https://www.nextadvance.com/bullet-blender-homogenizer/bullet-blender-models/
Thermo Orbitrap Eclipse MS system coupled to an Ultimate 3000 RSLC-Nano liquid chromatography system	Thermo Fisher Scientific	https://www.thermofisher.com/order/catalog/product/FSN04-10000
Thermo Orbitrap Lumos mass spectrometer coupled to an Ultimate 3000 RSLC-Nano liquid chromatography system	Thermo Fisher Scientific	https://www.thermofisher.com/order/catalog/product/IQLAAEGAAPFADBMBHQ

RESOURCE AVAILABILITY

Lead contact

Further information and requests for resources and reagents should be directed to and will be fulfilled by the lead contact, Anil Agarwal (anil.agarwal@utsouthwestern.edu).

Materials availability

Unique materials and reagents generated in this study are available upon request from the lead contact with a completed Material Transfer Agreement.

Data and code availability

- All data reported in this paper will be shared by the lead contact upon request.
- This paper does not report original code.
- Any additional information required to reanalyze the data reported in this paper is available from the lead contact upon request.

EXPERIMENTAL MODEL AND STUDY PARTICIPANT DETAILS

Mice of the same sex were randomly assigned to experimental groups. All animal studies were approved by the Institutional Use and Care of Animals Committee (IUCAC) at the University of Texas Southwestern Medical Center. All methods were performed in accordance with the relevant guidelines and regulations. All animals were kept in 12-h light/dark cycles at 22°C temperatures. Mice were fed either standard chow diet or doxycycline diet as indicated in the text. Both male and female mice were used for this study at 12 and 24 weeks of age.

The generation of Tg-$^{AT\text{-}hA2}$;$mA2^{-/-}$ mice[16] is described before and briefly below. The B6129F1 mouse line was obtained from Taconic Bioscience.

METHOD DETAILS

Brief description of generation of Tg-$^{AT\text{-}hA2}$;$mA2^{-/-}$ mice

Generation of transgenic AGPAT2 mouse model

To generate Tg-TRE-h*AGPAT2*, the human *AGPAT2* open reading frame (GenBank: NM_006412) was amplified with the following primers, including a Kozak sequence on the forward primer and XbaI restriction sites (underlined) on both primers for ease of cloning: Forward – 5′-GCTCTAGAGCCGCCACCATGGAGCTGTGGCCGTG-3′ and Reverse – 5′-GCTCTAGATCTACTGGGCCGGCTGCAC-3′. The amplified product was cloned into pDrive, then digested with XbaI to release the fragment. The fragment was then cloned in XbaI restricted pBluescript-TRE-Tight vector and h*AGPAT2* was Sanger sequenced to verify no PCR error occurred.

The strategy of linearizing this plasmid for injection with the recommended NaeI and SacII restriction sites was unusable because both sites are present in our h*AGPAT2* sequence. To overcome this difficulty, we designed primers to span the NaeI and SacII restriction sites of pBluescript-TRE-Tight-h*AGPAT2*, which were flanked by SpeI restriction sites (underlined). SpeI restriction sites are not present in the h*AGPAT2* sequence. Forward – 5′-GGACTAGTAGGGAAGAAAGCGAAAGGAG-3′; Reverse – 5′-GGACTAGTCTAAAGGGAACAAAAGCTGGA-3′.

The fragment was digested with SpeI and ligated into the same site into a vector of convenience for Sanger sequencing and amplification. Once the correct sequence was confirmed, the fragment was excised using SpeI, purified, and provided to the transgenic core at the University of Texas Southwestern Medical Center. The linearized plasmid was microinjected into C57BL/6J fertilized eggs.

Since we wanted to express hAGPAT2 only in adipose tissue, we crossed six male Tg-TRE-h*AGPAT2* mice with the Tg-*Adipo*-rtTA mouse line. The cross between these two lines produced a mouse strain expressing both h*AGPAT2* and rtTA protein (Tg-h*AGPAT2, Adipo*-rtTA). This mouse line, when fed doxycycline, would activate the expression of *AGPAT2* in adipose tissue.

To determine that these mice express h*AGPAT2*, we crossed six mice, and their progeny were genotyped for the presence of h*AGPAT2* and *rtTA*. Those mice that were positive for both transgenes were fed doxycycline (600 mg/kg) when they were 5–6 weeks old; the pellets were changed every alternate day for two weeks.

The expression of hAGPAT2 protein was further confirmed by immunoblot (Figure S1C). It is to be noted that the antibody raised against hAGPAT2[33] did not recognize mouse AGPAT2 protein (in-house experience). The immunoblot showed the presence of expressed hAGPAT2 in BAT and gonadal adipose tissue.

Generation of hAGPAT2 expression in mAgpat2$^{-/-}$ background

Upon confirming the expression of *AGPAT2* regulated by doxycycline, the Tg-h*AGPAT2, Adipo*-rtTA mice were crossed with m*Agpat2*$^{+/-}$ mice to generate Tg-h*AGPAT2, Adipo*-rtTA, m*Agpat2*$^{+/-}$ mice. The Tg-h*AGPAT2, Adipo*-rtTA, m*Agpat2*$^{+/-}$ mice were genotyped and these Tg-h*AGPAT2, Adipo*-rtTA, m*Agpat2*$^{+/-}$ heterozygous mice were crossed to generate Tg-h*AGPAT2, Adipo*-rtTA, m*Agpat2*$^{+/+}$, and Tg-h*AGPAT2, Adipo*-rtTA, m*Agpat2*$^{-/-}$ mice, which were used for subsequent experiments. The mating strategy to obtain experimental animals is shown in Figure S1D. This mouse strain is abbreviated hereafter as Tg-$^{AT\text{-}hA2}$;m*A2*$^{-/-}$.

Mouse genotyping

For genotyping of Tg-$^{AT\text{-}hA2}$;m*A2*$^{-/-}$ mice, we used primers to amplify the Tg-TRE-h*AGPAT2,* Tg-*Adipo*-rtTA, and m*Agpat2* alleles individually: Tg-TRE-h*AGPAT2:* forward 5′ – ATGGAGCTGTGGCCGTGTCT – 3′, reverse 5′ – AGTACTTGAAGCTTCGCACG – 3′, with a product size of 217 bp. Tg-*Adipo*-rtTA: Forward 5′ – GAACAACGCCAAGTCATTCCGCTG – 3′, reverse 5′ – CTCCTGTTCCTCCAATACGCAGCC – 3′ with a product size of 212 bp. Both the amplification products were confirmed by Sanger sequencing. *Agpat2*$^{-/-}$ mice used in this study have been described.[9] Mice were genotyped using the following allele discriminating primer sets: A15, CGG CTA GGT AAG CAG TTT GA; A8, AAA GCT GTG CCA GGG TGG GT; and S175, GAT TGG GAA GAC AAT AGC AGG CAT GC. Genomic DNA amplified with A15 + A8 will produce the WT allele of 733 bp and A8+S175 will produce the knockout allele of 614 bp.

Mouse genetic background testing

The genetic backgrounds of the generated Tg-$^{AT\text{-}hA2}$;m*A2*$^{-/-}$ mice and those of B6129F1 (abbreviated as B6/129) were tested using a Mouse Genome Scanning panel based on ~1113 SNPs (curated by Taconic Biosciences, Germantown, NY, USA) and selected specifically to highlight differences between inbred mouse strains. Taconic Biosciences conducted the mouse genetic background analysis. Additionally, B6/129 mice have been used primarily as a control for studies involving the use of targeted gene mutated mice on a mixed background originating from 129 ES cell-based chimeras that were subsequently mated to C57BL/6 mice. While they were not genetically identical to these mixed background targeted mutation mouse models, they approximate, in a consistent manner, the genetic mix that may be present in such models (https://www.taconic.com/mouse-model/b6129f1).

Oral glucose tolerance test (OGTT)

OGTT was performed in mice fasted for 6 h and then orally gavaged with D-glucose (2 g/kg body weight). Blood glucose (tail vein) was determined using a ReliOn blood glucometer (Walmart) immediately before the glucose gavage and at various time points after the administration of the glucose. Approximately 40 μL blood was collected from the tail vein in Microvette tubes (Sarstedt, Nümbrecht, Germany) containing clot activator. Tubes were spun at 10,000 x *g* for 5 min and serum was collected for insulin measurement. Serum insulin was measured by ELISA method (Crystal Chem, Downers Grove, IL, USA).

Insulin tolerance test (ITT)

ITT was performed in mice fasted for 3 h and then 1 U insulin/kg for female and 2 U insulin/kg for male was injected intraperitoneal (IP). Blood glucose (tail vein) was determined using a ReliOn blood glucometer (Walmart) immediately before the insulin given IP and at various time points after the administration of the insulin. The decrease in glucose level from time 0 is presented as percent decrease (Figure S7).

Homeostatic model assessment of insulin resistance (HOMA-IR)

The HOMA-IR was calculated using the formula HOMA-IR= (FPI x FPG)/22.5. Where FPI is fasting plasma insulin concentration (μU/ml) and FPG is fasting plasma glucose (mmol/L).

Indirect calorimetry

For indirect calorimetry, individual mice were placed in metabolic cages and acclimated for 72 h before the start of the experiments. The TSE LabMaster (TSE Systems GmbH, Gottmadingen, Germany) was used to collect data. Oxygen consumption (VO_2), carbon dioxide production (VCO_2), and total fluid and food intake were collected continuously over a 132 h period. The data was processed using CalR software developed by Amir I Mina and colleagues.[34]

Plasma metabolite measurements

Plasma triglyceride, glucose, and AST were measured using Dry-slide technology (Vitros 250 analyzer from Ortho Clinical Diagnostic (Raritan, NJ, USA)). All measurements were carried out at the Mouse Metabolic Phenotyping Core at University of Texas Southwestern.

Plasma insulin assay

Plasma insulin was measured by ELISA method (Crystal Chem, Downers Grove, IL, USA).

Triacylglycerol (TAG) assay

Liver triacylglycerol (TAG) was measured using a triglyceride colorimetric assay kit from Cayman chemical according to the manufacturer's protocol with a few minor adjustments. A known quantity of liver tissue (100 mg) and 25–50 mg adipose tissue was weighed and homogenized in 1 mL of the buffer with protease inhibitor (Roche, Basel, Switzerland). The tissue homogenate was first spun for (3000 x *g* for 10 min) to break the excessive froth and transferred to a microfuge tube and spun again at 10,000 x *g* for 10 min. The supernatant was transferred to another tube, including the fat layer, and the volume noted. A preliminary dilution of the samples allowed us to determine the dilution appropriate to be within the range of the standard. The TAG is expressed as mg/g tissue.

Total RNA isolation

A general method routinely used by us for total RNA extraction and RT-qPCR has been described before.[35,36] Briefly, total RNA was extracted from mouse liver tissues (~50–100 mg) using RNA STAT-60 (Tel-Test, Friendswood, TX, USA). RT-qPCR was carried out and analyzed as described below.

Reverse transcription quantitative polymerase chain reaction (RT-qPCR)

Total RNA, in equal quantity, was pooled from 2 to 6 samples of liver tissue of each genotype and sex, and RT-qPCR was carried out in a 20 μL reaction volume. A total of 1–20 μg RNA was DNase I treated using the DNase-free kit from Ambion (Grand Island, NY, USA). Complementary DNA was made using 1–2 μg DNase I-treated RNA using reverse-transcription kit from ABI (Carlsbad, CA, USA). RT-qPCR was performed in duplicate using 2.5 mM primers, 20 ng complementary DNA, and SYBR Green. All RT-qPCR were carried out in 96-well plates using the StepOnePlus real-time PCR system (Applied Biosystems, Foster City, CA, USA). RT-qPCR was performed twice in duplicate, and the transcript levels were normalized to *cyclophilin (cyclo)*. The ΔC_t value for each sample was calculated as $\Delta C_t = [C_t \text{ (gene of interest)} - C_t \text{ (}cyclo\text{)}]$. The $\Delta\Delta C_t$ value for each gene of interest was calculated as $\Delta\Delta C_t = [\Delta C_t \text{ (sample of interest)} - \Delta C_t \text{ (WT)}]$. The fold change was calculated as fold change = $2^{-\Delta\Delta Ct}$. Primers used for gene amplification were obtained from Harvard primer bank or were designed in-house and synthesized by Integrated DNA Technologies (Coralville, IA, USA), or were obtained from realtimeprimers.com (Elkins Park, PA, USA). Primers used in this study are provided in Table S3.

Quantitative PCR using pooled sample strategy

In a preliminary study, we amplified the expression of mRNA for several genes individually and in pooled samples and compared the raw C_t values for each gene. There is excellent correlation between the mean of individual samples to those when the samples are pooled.[35] We now routinely pool the samples for measurements of mRNA expression. Furthermore, in the current study, to account for the experimental variance, we generated cDNA from the pooled samples two different times and amplified independently in duplicates. To further reconfirm our pooling strategy, we performed a similar pooled test for three genes in the current liver samples and have found excellent correlation (see Table S4).

Tandem mass Tag-Mass Spectrometry (TMT-MS) for liver

Sample preparation

The TMT-MS method is described in detail in.[37] Approximately 40–70 mg liver samples were dispensed in snap cap 2 mL tubes and 500 μL of RIPA buffer (minus the Triton X-100) containing combined protease and phosphatase inhibitors cocktail. Approximately 150 mg of zirconium oxide beads were added to each tube and homogenized using a Bullet Blender according to the manufacturer's suggested protocol for liver tissue (Next Advance). The homogenates were centrifuged at 10,000 × g for 10 min at 4°C and the layer below the fat layer for those samples, which are from fatty liver, was transferred to another tube. The lysates were centrifuged again at the same speed and time and supernatant was saved in a clean tube to avoid any residual fat. The volume of tissue lysates was measured and appropriate quantity of 25% Triton X-100 was added to final concentration of 1%. The lysates were kept on ice for ~45–60 min and sonicated 3 × 5 s at 35% amplitude using Sonics Vibracell with cooling. The protein was measured using the DC assay kit and the lysate was used for TMT mass spectrometry as follows:

Peptide labeling and fractionation

Sodium dodecyl sulfate (SDS) was added to the tissue samples in RIPA buffer to bring it to a starting concentration of 3–5% SDS in 50 μL. Tris(2-carboxyethyl)phosphine (TCEP) was added to a final concentration of 20 mM and samples were incubated at 56°C for 30 min. After cooling, iodoacetamide was added to a final concentration of 20 mM and samples were incubated for 30 min at room temperature in the

dark. 50 μg samples were then transferred to S-Trap micro columns and digested overnight with 2 μg of trypsin at 37°C. Following digestion, the peptide eluate was dried and reconstituted in 100 mM triethylammonium bicarbonate (TEAB) buffer. The TMTpro 18plex Isobaric Mass Tagging Kit was used to label the peptides, as per the manufacturer's instructions. The labeled reactions were cleaned and fractionated using Pierce High pH Reversed-Phase Peptide Fractionation Kit into eight fractions according to the manufacturer's directions. The fractions were dried in a SpeedVac and reconstituted in a 2% acetonitrile, 0.1% Trifluoroacetic acid (TFA) buffer.

Phosphopeptide enrichment

Peptide samples were reconstituted with the binding buffer from the Thermo High-Select TiO_2 Phosphopeptide Enrichment kit. The pH of the samples was verified to be less than 3 using pH paper and were then loaded to TiO_2 Spin Tips for binding and washing. The flow through was collected for secondary enrichment with High-Select Fe-NTA Phosphopeptide enrichment columns (Thermo). The phosphopeptides collected from each enrichment step were combined, dried, and reconstituted in 2% (v/v) acetonitrile (ACN), 0.1% TFA in water. The unphosphorylated peptide fractions from each step were prepared the same way for analysis as well.

Peptide mass spectrometry

Peptides were analyzed on a Thermo Orbitrap Eclipse MS system coupled to an Ultimate 3000 RSLC-Nano liquid chromatography system. Samples were injected onto a 75 μm i.d., 75-cm long EasySpray column and eluted with a gradient from 0 to 28% buffer B over 180 min at a flow rate of 250 nL/min. Buffer A contained 2% (v/v) ACN and 0.1% formic acid in water, and buffer B contained 80% (v/v) ACN, 10% (v/v) trifluoroethanol, and 0.1% formic acid in water at a flow rate of 250 nL/min. Spectra were continuously acquired in a data-dependent manner throughout the gradient, acquiring a full scan in the Orbitrap [at 120,000 resolution with a standard automatic gain control (AGC) target] followed by MS/MS scans on the most abundant ions in 2.5 s in the ion trap (turbo scan type with an intensity threshold of 5,000, collisionally induced dissociation (CID) collision energy of 35%, standard AGC target, maximum injection time of 35 m and isolation width of 0.7 m/z). Charge states from 2 to 6 were included. Dynamic exclusion was enabled with a repeat count of 1, an exclusion duration of 25 s and an exclusion mass width of $\pm$10 ppm. Real-time search was used for selection of peaks for synchronous precursor selection-mass spectrometry to the third-MS3 (SPS-MS3) analysis, with searches performed against the mouse reviewed protein database from UniProt along with the sequence of human AGPAT2. Up to one missed tryptic cleavage was allowed, with carbamidomethylation (+57.0215) of cysteine and TMTpro reagent (+304.207) of lysine and peptide N-termini used as static modifications and oxidation (+15.9949) of methionine used as a variable modification. MS3 data were collected for up to 10 MS2 peaks that matched to fragments from the real-time peptide search identification, in the orbitrap at a resolution of 50,000, high-energy C-trap dissociation (HCD) collision energy of 65% and a scan range of 100–500 m/z, which allows a sufficient range of reporter ions to be detected.

Phosphopeptides mass spectrometry

Enriched phosphopeptides were analyzed on a Thermo Orbitrap Lumos mass spectrometer coupled to an Ultimate 3000 RSLC-Nano liquid chromatography system. Samples were injected onto a 75 μm i.d., 75-cm long EasySpray column and eluted with a gradient from 1 to 5% buffer B over 1 min and from 5 to 45% buffer B over 194 min at a flow rate of 250 nL/min. Buffer A contained 2% (v/v) ACN and 0.1% formic acid in water, and buffer B contained 80% (v/v) ACN, 10% (v/v) trifluoroethanol, and 0.1% formic acid in water at a flow rate of 250 nL/min. Spectra were continuously acquired in a data-dependent manner throughout the gradient, acquiring a full scan in the Orbitrap (at 120,000 resolution with a standard AGC target) followed by MS/MS scans on the most abundant ions in 3 s in the Orbitrap CID collision energy of 30%, standard AGC target, maximum injection time of 60 m. Multistage activation was performed with neutral loss mass of 97.9673. Charge states from 2 to 5 were included. Dynamic exclusion was enabled with a repeat count of 1, an exclusion duration of 25 s and an exclusion mass width of $\pm$10 ppm. SPS-MS3 data were collected in the Orbitrap for the 10 most intense MS2 peaks, in the orbitrap at a resolution of 50,000, HCD collision energy of 55%, a scan range of 100–500 m/z, normalized AGC target of 200%, and a maximum injection time of 120 ms.

Protein identification

Protein identification and quantification were done using Proteome Discoverer v.3.0 SP1. Raw MS data files were analyzed against the mouse reviewed protein database from UniProt along with the sequence of human AGPAT2. Both Comet and Sequest HT with INFERYS Rescoring were used, with carbamidomethylation (+57.0215) of cysteine and TMTpro reagent (+304.207) of lysine and peptide N-termini used as static modifications and oxidation (+15.9949) of methionine used as a variable modification. Reporter ion intensities were reported, with further normalization performed by using the total intensity in each channel to correct discrepancies in sample amount in each channel. The false-discovery rate (FDR) cutoff was 1% for all peptides.

Phosphopeptides identification and quantification

Phosphoprotein identification and quantification were done using Proteome Discoverer v.3.0 SP1. Raw MS data files were analyzed against the mouse reviewed protein database from UniProt along with the sequence of human AGPAT2. Sequest HT was used, with carbamidomethylation (+57.0215) of cysteine and TMTpro reagent (+304.207) of lysine and peptide N-termini used as static modifications, with oxidation (+15.9949) of methionine and phosphorylation (+79.966) of serine, threonine, and tyrosine used as variable modifications. Reporter ion

intensities were reported, with further normalization performed by using the same normalization factor as was used in the protein samples prior to phosphopeptide enrichment. The false-discovery rate (FDR) cutoff was 1% for all peptides.

QUANTIFICATION AND STATISTICAL ANALYSIS

No statistical methods were used to predetermine sample size. No method of randomization was used to determine how mice were allocated to experimental groups. Statistical methods used for each dataset are mixed model repeated measurements, Student's t test, one-way ANOVA, and one sample test. We determined the sex interaction for each experimental dataset to ascertain if the male and female data could be combined, which could improve the statistical power/effect. On occasion, we did observe a sex interaction, but not in all experimental datasets. Since there was no consistency in the sex interaction, we presented the male and female data separately. All analyses were performed using SAS 9.4 (SAS Institute, Cary, NC, USA). All statistical tests were two-sided, and $p < 0.05$ was considered as significant. Data were presented as mean $\pm$ SD except for the indirect calorimetry, where data are presented as mean $\pm$ SEM.